West African Monsoon water cycle: 2. Assessment of numerical weather prediction water budgets

Remi Meynadier, Olivier Bock, Sébastien Gervois, F. Guichard, J.-L. Redelsperger, A. Agustí-Panareda, A. Beljaars

West African Monsoon water cycle: 2. Assessment of numerical weather prediction water budgets

R. Meynadier,[1] O. Bock,[1,2] S. Gervois,[1] F. Guichard,[3] J.-L. Redelsperger,[3] A. Agustí-Panareda,[4] and A. Beljaars[4]

Received 22 January 2010; revised 27 May 2010; accepted 3 June 2010; published 1 October 2010.

[1] Water budgets from European Centre for Medium-Range Weather Forecasts (ECMWF) Re-Analysis (ERA)-Interim and National Centers for Environmental Prediction (NCEP) Reanalysis I and II are intercompared and compared to GPS precipitable water and to the 6 year hybrid budget data set described in part 1 of this study. Deficiencies are evidenced in the reanalyses which are most pronounced over the Sahel. Results from operational models (ECMWF Integrated Forecast System, NCEP Global Forecast System, and ARPEGE-Tropiques) and the special ECMWF African Monsoon Multidisciplinary Analyses reanalysis confirm and help understanding these findings. A bias (~1–2 mm d^{-1}) in precipitation and evapotranspiration leads to an unrealistic view of West Africa as a moisture source during the summer. North of the rainband (13°N–16°N), moisture flux convergence (MFC) shows a minimum in the NCEP models and divergence in the ECMWF models not consistent with the hybrid data set. This feature, added to presence of a deep layer of northerly dry air advected at midlevels (800–400 hPa), is thought to block the development of deep convection in the models and the northward propagation of the monsoonal rainband. The northerly flow is part of a shallow meridional circulation that is driven by the Saharan heat low. This circulation appears too strong in some of the models, a possible consequence of the too-approximate representation of physical processes and land surface properties over the Sahel. In most of the models, evapotranspiration shows poor connection with precipitation. This is linked with large analysis increments in precipitable water, soil moisture, and MFC. Despite the large biases affecting the water budget components in the models, temporal variations (seasonal and interannual) might nevertheless be recovered with reasonable accuracy.

Citation: Meynadier, R., O. Bock, S. Gervois, F. Guichard, J.-L. Redelsperger, A. Agustí-Panareda, and A. Beljaars (2010), West African Monsoon water cycle: 2. Assessment of numerical weather prediction water budgets, *J. Geophys. Res.*, *115*, D19107, doi:10.1029/2010JD013919.

1. Introduction

[2] Numerical weather prediction (NWP) models are often used for computing the atmospheric part of the water budget at global and regional scales [*Higgins et al.*, 1996; *Trenberth and Guillemot*, 1998; *Roads et al.*, 2002] but few studies consider specifically West Africa. Several past studies have pointed to significant deficiencies in the hydrological cycle represented in NWP model analyses and reanalyses [*Kanamitsu and Saha*, 1996; *Trenberth and Guillemot*, 1995, 1998; *Andersson et al.*, 2005; *Drusch and Viterbo*, 2007]. The deficiencies in NWP products can be due to a combination of deficiencies in physical parameterizations, in the assimilation schemes, and lack of or biases in observations. Radiosonde observations are a fundamental component of the upper air observing system since they are used as a reference to adjust biases in all the other observing systems [*Simmons et al.*, 2006]. Unfortunately, the Tropics are generally poorly covered with observational networks. Especially, the density of radiosonde stations in Africa is very sparse [*Parker et al.*, 2008]. Moreover, biases in these observations have been diagnosed [*Bock et al.*, 2007, 2008] and their impact on NWP products has been evidenced [*Bock and Nuret*, 2009; *Agustí-Panareda et al.*, 2009], It is thus not surprising that poor consensus emerged from the past water cycle studies over West Africa which used either NWP products or directly radiosonde data [*Lamb*, 1983; *Cadet and Nnoli*, 1987; *Brubaker et al.*, 1993; *Fontaine et al.*, 2003; *Bielli and Roca*, 2009].

[3] During the African Monsoon Multidisciplinary Analyses (AMMA) Special Observing Period (SOP) in summer 2006, many extra (conventional and research) observations were collected over West Africa [*Lebel et al.*, 2009]. A large number of this data was assimilated with operational NWP

[1]LATMOS, Université Pierre et Marie Curie, CNRS, Paris, France.
[2]Also at LAREG, IGN, Marne-la-Vallee, France.
[3]GAME–CNRM, CNRS, Météo-France, Toulouse, France.
[4]ECMWF, Reading, UK.

0148-0227/10/2010JD013919

Table 1. Main Characteristics of Numerical Weather Prediction Systems Used in This Study[a]

NWP Model	Assimilation System and Model Versions	Horizontal Resolution	Number of Vertical Levels (1000–100 hPa)	Analysis-Forecast Integration Times (*E* and *P*)
NCEP-NCAR Reanalysis I	3D-Var 10 Jan 1995	2.5° × 2.5° (upper air), ~1.9° × 1.9° (surface)	11 pressure levels	0000, 0600, 1200, 1800 UTC/0 to +6 hours
NCEP-DOE Reanalysis II	3D-Var 10 Jan 1995 improved	2.5° × 2.5° (upper air), ~1.9° × 1.9° (surface)	11 pressure levels	0000, 0600, 1200, 1800 UTC/0 to +6 hours
NCEP-GFS	3D-Var, 2006	1° × 1°	21 pressure levels	1200 UTC/+12 to +36 hours
ERA-Interim	4D-Var Cy31r1/2, Sep–Dec 2006	0.75° × 0.75°	26 pressure levels	1200 UTC/+12 to +36 hours
ECMWF-IFS	4D-Var Cy30r1, 1 Feb 2006; Cy31r1, 12 Sep 2006	0.25° × 0.25°	55 hybrid levels (starting 10 m above surface)	1200 UTC/+12 to +36 hours
ERA-AMMA	4D-Var Cy32r3, 6 Nov 2007	0.5° × 0.5°	55 hybrid levels (starting 10 m above surface)	0000, 1200 UTC/0 to +12 hours
ARPEGE-Tropiques	4D-Var 2006	0.5° × 0.5°	15 pressure levels	1200 UTC/+12 to +36 hours

[a]All the variables were available at a 6 hour time resolution. The last column reports the analysis times and forecast integration periods for *E* and *P* estimates. Abbreviations are as follows: AMMA, African Monsoon Multidisciplinary Analyses; ARPEGE, Action de Recherche Petite Echelle Grande Echelle; DOE, U.S. Department of Energy; ECMWF, European Centre for Medium-Range Weather Forecasting; ERA, ECMWF Re-Analysis; GFS, Global Forecasting System; NCAR, National Center for Atmospheric Research; NCEP, National Centers for Environmental Prediction; NWP, numerical weather prediction.

systems. There is thus a significant interest in evaluating NWP products during this special period in comparison to the past. Another interest and motivation for this work is the evaluation of the new ECMWF reanalysis, ERA-Interim [*Simmons et al.*, 2006], and the special ECMWF AMMA reanalysis (A. Agustí-Panareda et al., The ECMWF reanalysis for the AMMA observational campaign, submitted to *Quarterly Journal of the Royal Meteorological Society*, 2009, hereafter referred to as Agustí-Panareda et al., submitted manuscript, 2009). The former is investigated here over period 2002–2007, and compared to the NCEP reanalyses and to the hybrid data set [*Meynadier et al.*, 2010]. The latter covers only the period from 1 May to 30 September 2006. It will be compared over that period to operational NWP products (ECMWF Integrated Forecast System (IFS), NCEP Global Forecast System (GFS), and ARPEGE-Tropiques). Compared to past ECMWF and NCEP reanalyses, ERA-Interim and the AMMA reanalysis are produced with a 4D-Var assimilation system and more recent physics (see Table 1). In the AMMA reanalysis, the radiosonde data are corrected for dry humidity biases before they are assimilated [*Agustí-Panareda et al.*, 2009]. A simplified version of this correction scheme is also used operationally at ECMWF.

[4] The present paper is the second part of a study focused on the regional-scale water cycle of the West African Monsoon in the framework of AMMA. In part 1, we investigated the annual mean water budgets, the seasonal cycle and interannual variability. This analysis was carried out with a hybrid data set of water budget terms based on an ensemble of nine Land Surface Model simulations forced with elaborate precipitation and radiation products derived from satellite observations over the period 2002–2007. Vertically integrated atmospheric moisture flux convergence was estimated as a residual from the water budget equation at the surface. This approach provided accurate and consistent water budget terms, such as surface evapotranspiration, rainfall, and atmospheric moisture flux divergence (MFD). It revealed several limiting and controlling factors, and suggested a strong sensitivity of the regional water cycle to atmospheric dynamics and surface radiation.

[5] The main motivation of the present study is to assess the capacity of NWP model reanalyses to simulate the functioning of the water cycle of West Africa in a way consistent with the hybrid data set. The NWP products provide also a description of the three-dimensional distribution of atmospheric circulation and moisture fluxes, and potentially of vertically resolved water budget terms [*Trenberth and Smith*, 2009]. Moreover, the reanalyses allow for investigating multidecadal time periods of pertinence when investigating interannual variability.

[6] The organization of the paper is the following. Section 2 describes the data, methods and error sources in the computation of MFD from gridded model data. The evaluation of the errors is detailed in the Appendix A. Section 3 focuses on the assessment of the water budget provided by NWP reanalyses over the 6 year period covered by the hybrid data set. Section 4 investigates in more details the uncertainties and deficiencies evidenced in the reanalyses with the help the AMMA reanalysis and operational models. Namely, important features of regional-scale atmospheric circulation are highlighted. Section 5 discusses the results and provides conclusions.

2. Data, Methods, and Error Sources

[7] The vertically integrated atmospheric water budget equation can be expressed as

$$\frac{\partial}{\partial t}\frac{1}{g}\int q dp + \nabla \cdot \frac{1}{g}\int qV dp = E - P, \tag{1}$$

where E is the evapotranspiration from the surface, P is the precipitation at the surface, q is the specific humidity in the atmosphere at pressure level p, and V is the horizontal wind velocity vector at pressure level p. The vertical integrals are assumed to extend over the whole atmosphere, i.e., from the surface, at pressure, p_s, to some upper pressure level, p_t, where specific humidity is assumed to vanish. The first term on the left-hand side represents the precipitable water vapor (PWV) tendency, denoted dPW in the following, and the second term represents the moisture flux divergence, referred to as MFD. Hence, equation (1) can be rewritten as follows:

$$\mathrm{dPW} + \mathrm{MFD} = E - P. \tag{2}$$

NWP systems provide estimates for all terms intervening in equation (1) or (2). E and P are simulated (forecast) variables. They are usually cumulated during the simulation and correspond to time-integrated quantities; dPW is computed from the archived PWV contents. MFD is computed offline from q and V (equation (1)), available either on model levels or pressure levels, or both. The model fields used for the computation of MFD and dPW are instantaneous quantities available at a time interval of 6 hours. These are then combined to form daily mean quantities:

$$\mathrm{MFD_{daily}} = 1/8\ \mathrm{MFD_{00}} + 1/4\ \mathrm{MFD_{06}} + 1/4\ \mathrm{MFD_{12}} + 1/4\ \mathrm{MFD_{18}} + 1/8\ \mathrm{MFD_{24}} \quad (3)$$

$$\mathrm{dPW_{daily}} = \mathrm{PWV_{24}} - \mathrm{PWV_{00}}. \quad (4)$$

When analyzing water budgets produced with NWP assimilation systems (reanalyses as well as operational forecasts and analyses), one has to be careful about a number of limitations. First, there are discontinuities in the time evolution of the various fields which are introduced by the assimilation of observations. This is a necessary step to avoid the model forecasts to drift toward the model's climatology which is usually different from the real world because of limitations in physical parameterizations and other approximations and assumptions in the model. Over West Africa, the most prominent problems in global circulation models are north-south displacements in the mean atmospheric circulation patterns [*Tompkins et al.*, 2005], the rainbelt [*Hourdin et al.*, 2010] and the associated moist air mass [*Nuret et al.*, 2008; *Bock et al.*, 2008] and surface fluxes [*Boone et al.*, 2009b]. For the assimilation step, a short-term forecast is used as first guess. However, models drift and observations contain errors. Hence the assimilation system has to deal with inconsistencies between the first guess and the observations. This leads to large increments and unrealistically active adjustments in the subsequent forecasts commonly referred to as spin-up or spin-down effects [*Betts et al.*, 1999; *Andersson et al.*, 2005]. The quality of a particular model variable depends thus on how much it relies on physical parameterizations and on assimilated observations. Variables such as E and P are least accurate because they depend heavily on physical parameterizations. Humidity and wind fields are more accurate because they are constrained by the assimilation of observations (mostly radiosondes). However, biases in the observations directly impact the analyzed fields and enhance spin-up–spin-down effects. Specifically for West Africa, *Bock et al.* [2007] and *Bock and Nuret* [2009] used independent GPS data and diagnosed dry and wet biases in radiosonde data and in NWP model analyses and reanalyses having assimilated those observations.

[8] Second, the closure of the water budget equation and the balance between terms will be different when considering either purely forecast fields or when mixing forecast (FC) and analysis (AN) fields. The FC budget is in principle closed, i.e., $\mathrm{dPW_{FC}} + \mathrm{MFD_{FC}} = E_{\mathrm{FC}} - P_{\mathrm{FC}}$, whereas a mix of AN and FC budget terms is not, $\mathrm{dPW_{AN}} + \mathrm{MFD_{AN}} \neq E_{\mathrm{FC}} - P_{\mathrm{FC}}$, because of the analysis increments. Some authors have included the analysis increments in one of the budget term (e.g., dPW) to deal with a closed budget [e.g., *Higgins et al.*, 1996]. In the present study we did not introduce such a correction, but rather quantify the imbalance as it reveals inconsistencies between the model and observations. Since any particular NWP model uses a particular set of physical parameterizations, numerical schemes, and assimilation procedures, an intercomparison of several NWP model products is useful to assess the uncertainties and limitations associated with these features. Two distinct closure errors will be of interest: (1) the residual of the combination of AN and FC terms from the NWP systems,

$$\mathrm{Res}_a = \mathrm{dPW_{AN}} + \mathrm{MFD_{AN}} - E_{\mathrm{FC}} + P_{\mathrm{FC}}, \quad (5)$$

and (2) the residual of the combination of the AN terms with the hybrid data:

$$\mathrm{Res}_b = \mathrm{dPW_{AN}} + \mathrm{MFD_{AN}} - E_{\mathrm{ALMIP}} + P_{\mathrm{TRMM}}. \quad (6)$$

Third, the computation of MFD such as defined by equations (1) and (3) is known to suffer from a number of computational errors, independently of the accuracy of the wind and humidity fields [*Trenberth*, 1991]. These imply the vertical resolution, the treatment of variables near the surface, and time sampling. In the case of pressure-level data (obtained through postprocessing of model-level variables), the vertical integral of mass is usually not conserved. Coarse horizontal and vertical resolutions may enhance errors in the computation of horizontal divergence from finite differences near the surface, especially in regions of steep orography and/or marked by low-level jets [*Trenberth and Guillemot*, 1995; *Higgins et al.*, 1996]. Time sampling is an issue in regions with marked diurnal cycle in atmospheric circulation. West Africa obviously presents many of these characteristics [*Parker et al.*, 2005; *Lothon et al.*, 2008; *Bock et al.*, 2008].

[9] Note that, by using forecast terms in the water budget equation (equation (5)) becomes: $\mathrm{Res}_a = \mathrm{dPW_{AN}} + \mathrm{MFD_{AN}} - (\mathrm{dPW_{FC}} + \mathrm{MFD_{FC,cumul}})$, where $\mathrm{MFD_{FC,cumul}} = E_{\mathrm{FC}} - P_{\mathrm{FC}} - \mathrm{dPW_{FC}}$ is derived as a residual and therefore it is not subject to the computational errors described above (see the Appendix A). Hence, Res_a is a combination of analysis increments (AN – FC differences) and computational errors associated with $\mathrm{MFD_{AN}}$. Similarly, introducing the water budget equation for the hybrid data set, $\mathrm{MFD_{hyb}} = E_{\mathrm{ALMIP}} - P_{\mathrm{TRMM}} - \mathrm{dPW_{AN,}}$ equation (6) becomes: $\mathrm{Res}_b = \mathrm{MFD_{AN}} - \mathrm{MFD_{hyb}}$. Hence, Res_b quantifies the error associated with $\mathrm{MFD_{AN}}$ with respect to $\mathrm{MFD_{hyb}}$. It includes both computational errors in $\mathrm{MFD_{AN}}$ and analysis errors in the gradients of wind and moisture.

[10] The Appendix A provides a comprehensive assessment of these error sources for the ECMWF Integrated Forecast System (ECMWF-IFS) which are believe to be representative of state-of-the-art NWP systems. The following results are found for averages over areas of several 10^6 km^2:

[11] 1. Apart from computational errors, when MFD is estimated directly from q and V fields, the FC budget is closed.

[12] 2. The FC budget, though being closed, reveals large and unrealistic $\mathrm{dPW_{FC}}$ values, associated with significant drifts and spin-up–spin-down effects in the model compared

to GPS observations. This suggests that the other FC budget terms should also be interpreted with care.

[13] 3. In contrast, dPW_{AN} is more accurate, and MFD_{AN} is expected to more accurate too (it will be assessed in the following section with the hybrid data set).

[14] 4. The analysis increment for dPW + MFD explains most of the residual (Res_a) when AN and FC terms are mixed. It shows a bias of −0.9 to −1.6 ± 0.5 mm d^{-1} for monthly estimates.

[15] 5. The computational errors, combined of time sampling error due to the use of 6 hourly fields and the approximation of the divergence operator with a finite difference method, are evaluated to ± 0.5 mm d^{-1} (RMS) for monthly MFD estimates.

[16] 6. Using pressure level data instead of model level data and/or coarse horizontal resolutions enhances significantly the computational errors (e.g., bias of −0.3 to +1.0 mm d^{-1} with 10 pressure level data).

[17] In section 3 water budget terms from three NWP model reanalyses are intercompared and compared to the hybrid data set [*Meynadier et al.*, 2010] over the period 2002–2007. The NWP model reanalyses are: ERA-Interim [*Simmons et al.*, 2006], NCEP reanalysis I (referred to as NCEP-R1 [*Kalnay et al.*, 1996]) and NCEP reanalysis II (referred to as NCEP-R2 [*Kanamitsu et al.*, 2002]). It is useful to recall here that the hybrid data set is composed of evapotranspiration from AMMA Land surface Model Intercomparison Project (ALMIP [*Boone et al.*, 2009a]), rainfall from Tropical Rainfall Measuring Mission (TRMM) 3B42 satellite product [*Huffman et al.*, 2007], and PWV tendency from ERA-Interim reanalysis, and that MFD is obtained residually using the water budget equation (2). Compared to direct calculation of MFD from NWP models' gridded data, the hybrid MFD is exempt of numerical errors. This difference may contribute to the discrepancy observed between both estimates.

[18] In section 4, the ECMWF AMMA reanalysis (referred to as ERA-AMMA) (Agustí-Panareda et al., submitted manuscript, 2009) and three operational models, ECMWF-IFS, NCEP Global Forecast System (NCEP-GFS), and ARPEGE-Tropiques are also considered. Table 1 summarizes major characteristics of these products. Further information about NCEP-GFS can be found at http://www.emc.ncep.noaa.gov/gmb/moorthi/gam.html and about ECMWF-IFS at http://www.ecmwf.int/research/ifsdocs/.

[19] The budget terms will be quantified in three boxes representative of the West African climate: the Guinean (GUI) box, the Sudanian (SOU) box, and the Sahelian (SAH) box (see Figure 1). Note that the southern boundary of the GUI box used here is 7.5°N. It was shifted to the north compared the one used by *Meynadier et al.* [2010] to fit the coarser horizontal resolution of the NCEP reanalyses.

3. Water Budget From NWP Model Reanalyses

3.1. Spatial Distribution of Water Budget Terms

[20] Figure 1 shows the annual mean P, E, and E-P from the hybrid data set and the three NWP model reanalyses over the period 2002–2007. P and E for the reanalyses are presented as differences with respect to the hybrid data set. These variables exhibit a large meridional gradient over West Africa with a nearly zonal distribution between 10°N and 20°N. In the annual mean, the hybrid data set shows that West Africa is a sink area for atmospheric moisture ($E_{ALMIP} - P_{TRMM} < 0$) in the Sudano-Guinean region, while the budget is neutral ($E_{ALMIP} - P_{TRMM} \sim 0$) in the Sahel. The Sudano-Guinean region is thus characterized by an exoreic hydrologic regime with a significant part of rainfall escaping in runoff, while the Sahelian region is predominantly endoreic, i.e., nearly all surface rainfall is reevaporated in the atmosphere.

[21] Overall, the latitudinal gradients in P and E are much too steep in the reanalyses. Precipitation is not sufficiently far north compared to TRMM precipitation, reaching at least 20°N, and all three reanalyses show biases in P up to 250 mm between 10°N and 15°N. Large negative biases (up to 500 mm) are also seen in the maximum precipitation area of the Cameroun highlands and the Nigerian plateau. On the other hand, the reanalyses show an excess of precipitation along the Gulf of Guinea until 10°N, especially over the Fouta-Djalon Mountains (10°W, 8°N). The reanalyses show also biases in evapotranspiration, in comparison to the ALMIP product, with positive biases (E in excess) in the Soudano-Guinean region and negative biases (deficit in E) in the Sahelian region, except for NCEP-R2. In all three reanalyses, E-$P > 0$ in the Sudano-Sahelian region (roughly, north of 10°N), i.e., the opposite of what is obtained from the hybrid data set. These features reveal significant caveats in the NWP models that are partly reflected in a too southerly rainbelt, but not only.

[22] Table 2 provides a more quantitative insight into the biases in the three latitudinal bands. In the GUI box, the P excess in the reanalyses ranges from 81 mm (7%, ERA-Interim) to ~537 mm (47%, NCEP-R1), while in the SAH box, the P deficit ranges from 186 mm (72%, ERA-Interim) to 195 mm (76%, NCEP-R1). In the SOU box, ERA-Interim performs very poorly compared to the NCEP reanalyses. In all three reanalyses, $E > P$ in the SOU and SAH boxes, which implies that the physical link between E and P is not properly modeled in these regions, especially in the Sahel where the vegetation quickly dries out after the monsoon and precipitation is the only source of soil moisture at this scale [*Descroix et al.*, 2009].

[23] The link between E and P is further investigated with scatterplots in Figure 2, where both the annual mean values and 6 year averages are plotted. Interannual variability introduces some scatter around the 6 year averages but does not change the main interpretations that can be derived from the averages. In the SAH box, the hybrid data set shows a fairly linear relationship, between P_{TRMM} and E_{ALMIP}, whereas in the SOU box, saturation occurs around E_{ALMIP} = 800 mm. A broad scatter is seen in the GUI box, with annual mean E_{ALMIP} values lying in the range 600–1000 mm. In contrast, the reanalyses show a significantly different E-P relationship. In the SAH box, and most of the SOU box, $E > P$ for all values of P. In ERA-Interim, in particular, this indicates that there is no limiting control of rainfall on evapotranspiration. In both NCEP reanalyses, the relationship between E and P is more linear and closer to the 1:1 line, both in the SAH and SOU boxes. The upper limit of E in these reanalyses is also more reasonable compared to the ALMIP simulations. In the SOU box, the three reanalyses reveal saturation in evapotranspiration, in regions where P reaches 1000–1200 mm. But E is in excess everywhere compared to

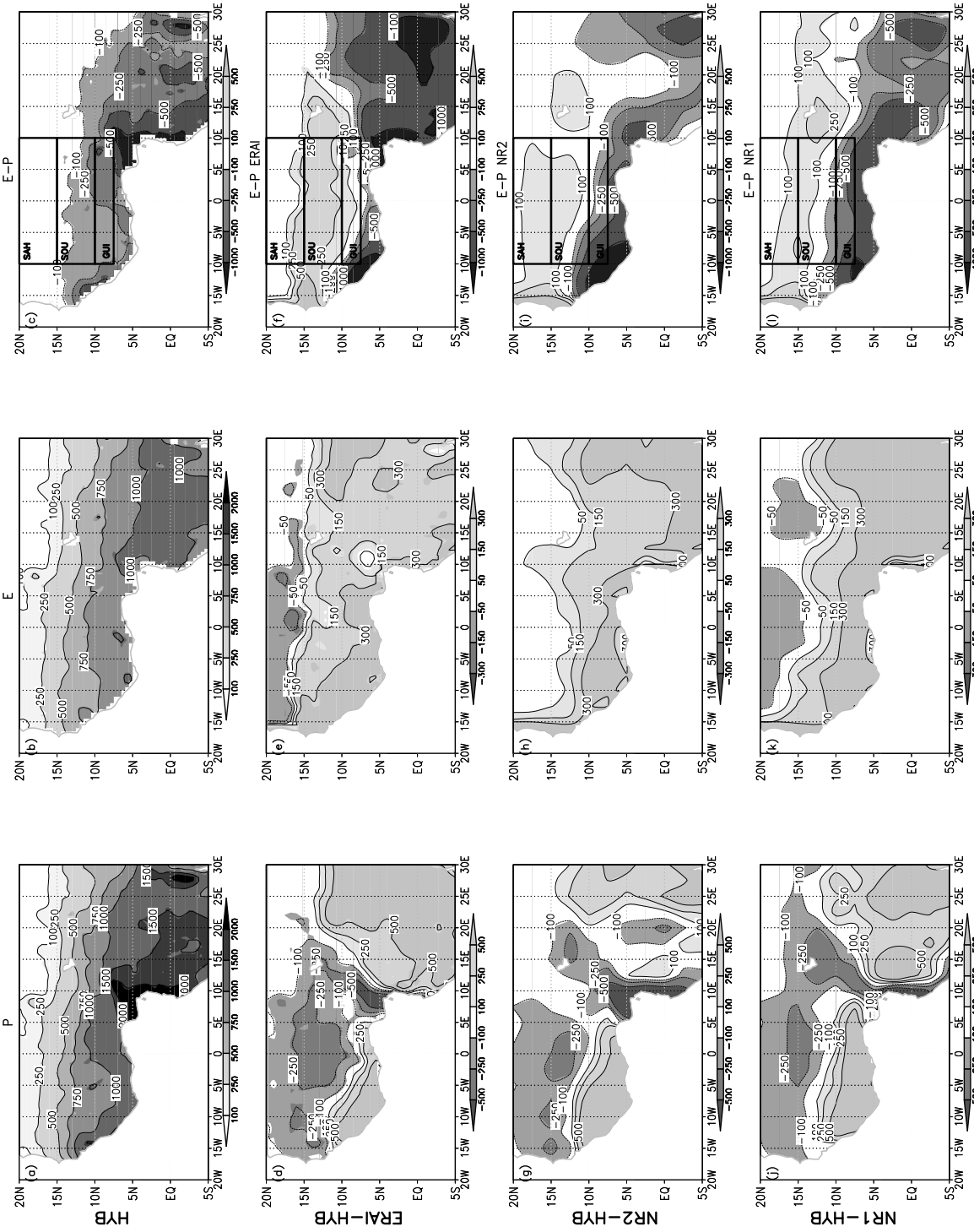

Figure 1. Annual mean (a) precipitation, (b) evapotranspiration, and (c) evapotranspiration minus precipitation for the hybrid data set (TRMM 3B42 precipitation and ALMIP multimodel evapotranspiration). (d, e, g, h, j, k) Precipitation and evapotranspiration for ECMWF ERA-Interim, NCEP-R1, and NCEP-R2 are presented as differences with respect to the hybrid data set. (f, i, l) Evapotranspiration minus precipitation for the three reanalyses. The data are averaged over years 2002–2007. Units are mm yr^{-1}.

Table 2. Annual Mean of *P*, *E*, and MFD Terms in Three Boxes (GUI, SOU, SAH) for the Same Four Data Sets as in Figure 1; Standard Deviation of Monthly Mean Anomalies; and Correlation Coefficients Between Monthly Mean Anomalies From the Hybrid Data Set and the NWP Reanalyses[a]

	GUI			SOU			SAH		
	P	*E*	MFD	*P*	*E*	MFD	*P*	*E*	MFD
				Annual Mean (mm yr^{-1})					
Hyb	1136	823	−313	717	547	−141	257	224	−32
ERAI	1217	1139	−312	524	772	98	71	192	0
NCEP-R2	1521	1143	−816	675	713	−521	103	224	−120
NCEP-R1	1673	1242	−1001	671	710	−504	62	160	−167
				Standard Deviation of Monthly Anomalies (mm month^{-1})					
Hyb	21	6	21	17	5	17	7	4	8
ERAI	15	4	25	11	4	17	3	2	9
NCEP-R2	37	6	32	18	5	21	8	4	12
NCEP-R1	24	6	28	15	3	18	4	1	8
				Correlation Coefficient of Monthly Anomalies					
ERAI	0.26[b]	0.55[c]	0.37[c]	0.71[c]	0.42[c]	0.48[c]	0.69[c]	0.63[c]	0.73[c]
NCEP-R2	0.45[c]	0.39[c]	0.55[c]	0.58[c]	0.56[c]	0.36[c]	0.72[c]	0.81[c]	0.61[c]
NCEP-R1	0.21	0.01	0.35[c]	0.30[b]	0.11	0.25[b]	0.55[c]	0.45[c]	0.53[c]

[a]Abbreviations are as follows: ERA, ECMWF Re-Analysis; MFD, moisture flux divergence; NCEP, National Centers for Environmental Prediction.
[b]Correlations tested at the two-sided 0.1 level using a random-phase test [*Ebisuzaki*, 1997].
[c]Correlations tested at the two-sided 0.05 level using a random-phase test [*Ebisuzaki*, 1997].

ALMIP. In the GUI box, the bias in *E* appears broadly as resulting from a translation toward larger values in *E* and *P*.

[24] A twofold deficiency is thus diagnosed in these reanalyses: a significant deficit in precipitation in the Sudan-Sahel and an excess of evapotranspiration in the same region, except to the very north (Figure 1). *Fontaine et al.* [2003] reported similar conclusions over a longer time period with NCEP-R1, especially $E > P$ over the Sahel. *Nuret et al.* [2007] and *Agustí-Panareda et al.* [2009] also noticed an insufficient northward penetration of the rainbelt over the Sahel in the ECMWF short-range forecasts. The first deficiency might be due to inaccurate convection schemes or large-scale features not favorable to the initiation of convection (e.g., dry air). This deficiency may be further diagnosed by inspecting MFD (see below), since a strong relationship between precipitation and moisture convergence has been highlighted by *Meynadier et al.* [2010]. The second deficiency can be due to the surface scheme and/or the soil moisture analysis scheme. Here significant differences are seen between the three reanalyses (Figure 2). Indeed, soil moisture is analyzed in very different ways in these models. In ERA-Interim, the soil moisture analysis is based on a short-range model forecast (first guess) and screen-level variables (2 m temperature and 2 m relative humidity [*Drusch and Viterbo*, 2007]), similarly to ECMWF-IFS. While ECMWF-IFS performs well globally, large soil moisture increments have been reported by Agustí-Panareda et al. (submitted manuscript, 2009) over West Africa in response to large first guess minus observation departures. These may in turn explain errors in evapotranspiration and in the precipitation forecast. The soil moisture analysis scheme is very different in NCEP-R2 reanalysis [*Kanamitsu et al.*, 2002]. The increment is scaled to the difference between 5 day pentad precipitation from a short-range model forecast and a reference precipitation product based on observations (CMAP). In contrast to the previous analysis scheme, the latter can potentially correct a deficit in modeled precipitation. Such a feature could explain why $E_{\mathrm{NCEP-R2}} \sim E_{\mathrm{ALMIP}}$ north of 16°N. In NCEP-R1, the procedure is similar but the reference soil moisture product is given by a climatology data set [*Kalnay et al.*, 1996]. In both NCEP reanalyses, scaling soil moisture increments with a reference precipitation product has also the advantage of limiting the rate of evapotranspiration to reasonable values [*Maurer et al.*, 2001].

[25] The balance between $E_{\mathrm{FC}} - P_{\mathrm{FC}}$ and $\mathrm{MFD_{AN}}$, and the difference between $\mathrm{MFD_{AN}}$ and $\mathrm{MFD_{hyb}}$, are investigated from Table 2 at the annual mean time scale. Here it is important to recall that $E_{\mathrm{FC}} - P_{\mathrm{FC}}$ is obtained from forecast variables, whereas $\mathrm{MFD_{AN}}$ is computed from 6 hourly, analyzed, wind and humidity fields, and $\mathrm{MFD_{hyb}}$ is obtained as a residual from the hybrid data set. A perfect balance between $E_{\mathrm{FC}} - P_{\mathrm{FC}}$ and $\mathrm{MFD_{AN}}$ is not expected because of computational errors in $\mathrm{MFD_{AN}}$ and analysis increments (see section 2). Table 2 shows that the discrepancy between $E_{\mathrm{FC}} - P_{\mathrm{FC}}$ and $\mathrm{MFD_{AN}}$ can be very large (121–234 mm for ERA-Interim, 241–559 mm for NCEP-R2, and 265–570 mm for NCEP-R1) and beyond the assumed uncertainty in $\mathrm{MFD_{AN}}$ (see the Appendix A) It is seen that $E_{\mathrm{FC}} - P_{\mathrm{FC}} > \mathrm{MFD_{AN}}$ in all three boxes, for all three reanalyses. This discrepancy is therefore mostly due to the biases in E_{FC} and P_{FC} discussed above. One must also notice that, whereas $\mathrm{MFD_{hyb}} < 0$ in all three boxes (consistently with the fact that $E_{\mathrm{ALMIP}} - P_{\mathrm{TRMM}} < 0$), ERA-Interim has the opposite sign ($\mathrm{MFD_{ERAI}} > 0$) in the SOU and SAH boxes. This bias in $\mathrm{MFD_{ERAI}}$ is connected with the bias in P_{ERAI} as will become evident below. Comparatively, the NCEP reanalyses show a more consistent water budget in the SOU and SAH boxes, despite a bias present there as well.

[26] Figure 3 provides more insight into the spatial distributions of *P* and MFD, on average over June to September 2002–2007. A strong link is seen between $\mathrm{MFD_{hyb}}$ and P_{TRMM}, with coincident isolevels (P_{TRMM} = 150/90/30 mm with $\mathrm{MFD_{hyb}}$ = 75/30/10 mm) throughout West Africa. The three reanalyses display quite different patterns and relationships. Most striking is the pattern of moisture divergence in ERA-Interim ($\mathrm{MFD_{ERAI}} > 0$), centered on 13°N–15°N. Divergence is observed also in NCEP reanalyses,

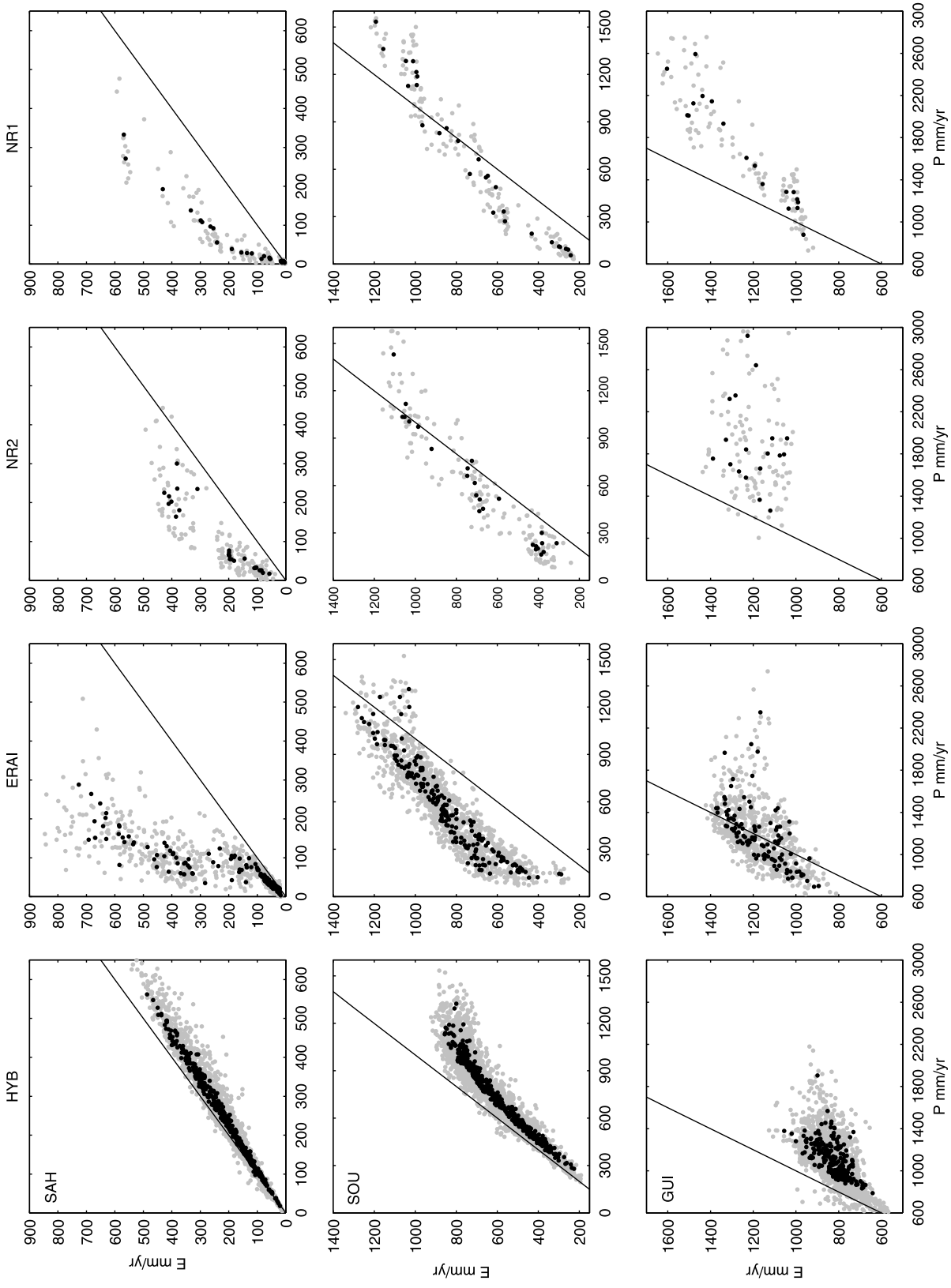

Figure 2. Scatterplots of annual mean evapotranspiration versus precipitation for the grid points located in the three domains indicated in Figure 1: (top) SAH box, (middle) SOU box, and (bottom) GUI box. Individual years are plotted in shading, and the 6 year average is in black. Units are mm yr^{-1}.

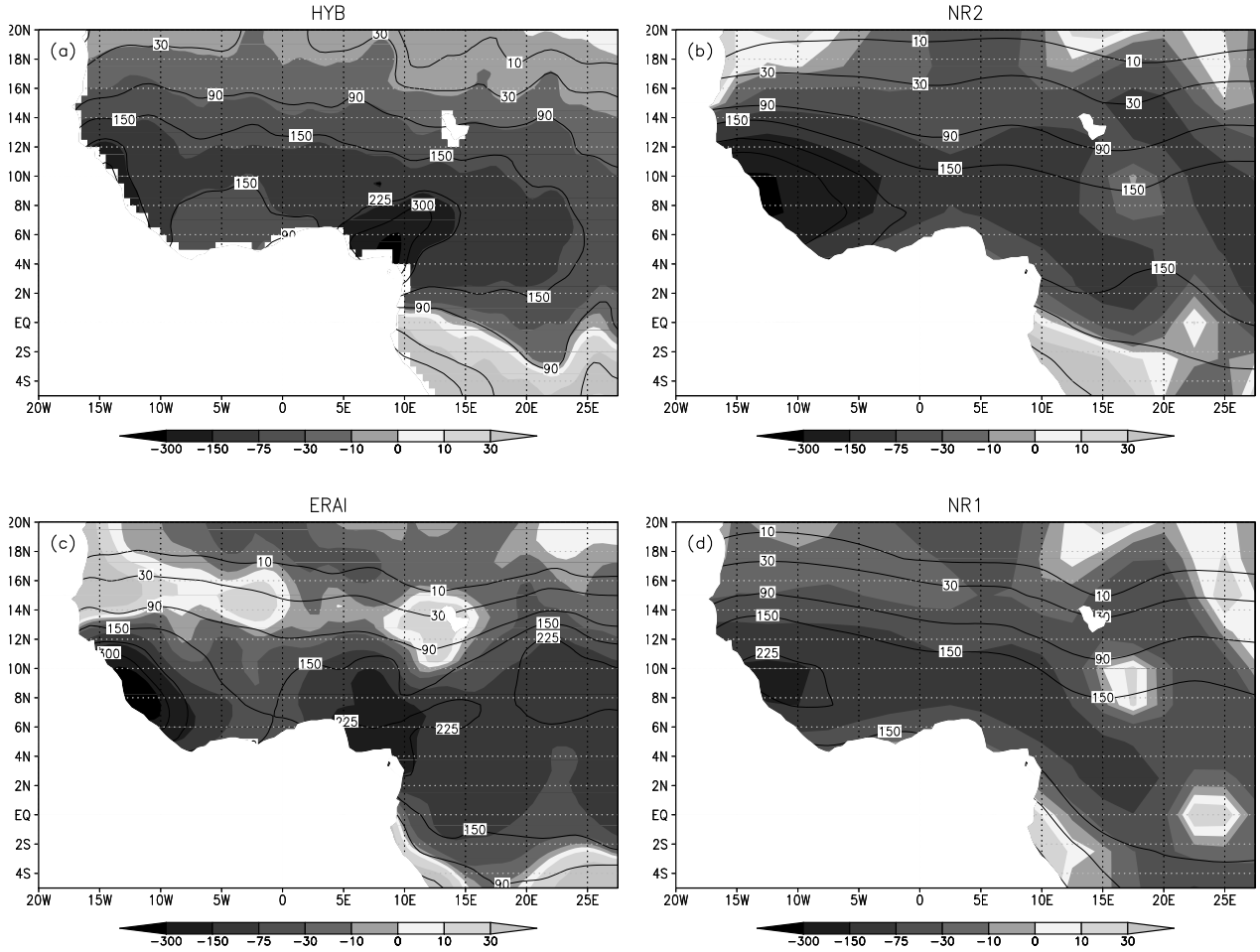

Figure 3. Moisture flux divergence (shaded) and precipitation (contours) averaged from June to September 2002–2007 for (a) the hybrid data set, (b) NCEP-R2, (c) ERA-Interim, and (d) NCEP-R1. Units are mm month^{-1}.

but it is located more northward (above 18°N, around 10°W and 15°E; and around 8°N–17°E in NCEP-R1). All three reanalyses show a drop in P_{FC} in the vicinity of patterns of moisture divergence (ERA-Interim) or reduced moisture convergence (NCEP). This raises the question of the origin and possible role of the reduced moisture convergence-divergence patterns in the too southerly position of the rain-belt seen in all three reanalyses. It is also possible that the too strong evapotranspiration favors the occurrence of moisture divergence.

[27] It is also worth noting that in Figure 3 there are consistent patterns in MFD_{AN} and P_{FC} in all three reanalyses south of 13°N (e.g., there is a good correspondence between P_{FC} = 150 mm and MFD_{AN} = −75 mm). However, north of 16°N, all three reanalyses show a region of increased moisture convergence which is not present in MFD_{hyb}. This feature occurs in the region of the intertropical discontinuity (ITD) and may be linked to stronger mass convergence in the models (see section 4) but also to increased computational errors in the MFD_{AN} estimates (e.g., due to a marked diurnal cycle in low-level moisture transport).

3.2. Seasonal Evolution of Water Budget Terms

[28] Figure 4 shows the seasonal evolution of moisture budget terms. In all three boxes, the three reanalyses show a distinct seasonal cycle in E_{FC} and P_{FC}, rather well in phase with E_{ALMIP} and P_{TRMM}, but significant biases are evident. In the SAH box, large negative biases are observed in both terms during the monsoon season, with a bias in P_{FC} up to 2 mm d^{-1} in August. The reanalyses display a very flat seasonal cycle of $E_{FC} - P_{FC}$ compared to $E_{ALMIP} - P_{TRMM}$. In the SOU box, the seasonal cycle of E_{FC}, P_{FC}, and $E_{FC} - P_{FC}$ in the reanalyses is slightly better. However, NCEP-R2 has a deficit of rainfall in May–June, NCEP-R1 has an excess of rainfall in September–November, and ERA-Interim has a deficit in rainfall during the whole season (April–September). E_{FC} is overestimated during the dry season in NCEP-R2 and ERA-Interim, and during the wet season in NCEP-R1. In the GUI box, P_{ERAI} fits quite well with P_{TRMM}, whereas both NCEP reanalyses show an excess of rainfall that reaches 3–4 mm d^{-1} in August. In NCEP-R1, the bias remains until the end of the year. All three reanalyses provide E_{FC} values in excess of around 1 mm all year long. The seasonal evolution of $E_{FC} - P_{FC}$ from ERA-Interim is the closest to $E_{ALMIP} - P_{TRMM}$, whereas both NCEP reanalyses have larger errors.

[29] All three reanalyses show a marked seasonal cycle in MFD_{AN} in all three boxes, in rather good consistency with MFD_{hyb} but in contrast with their $E_{FC} - P_{FC}$ budget. A

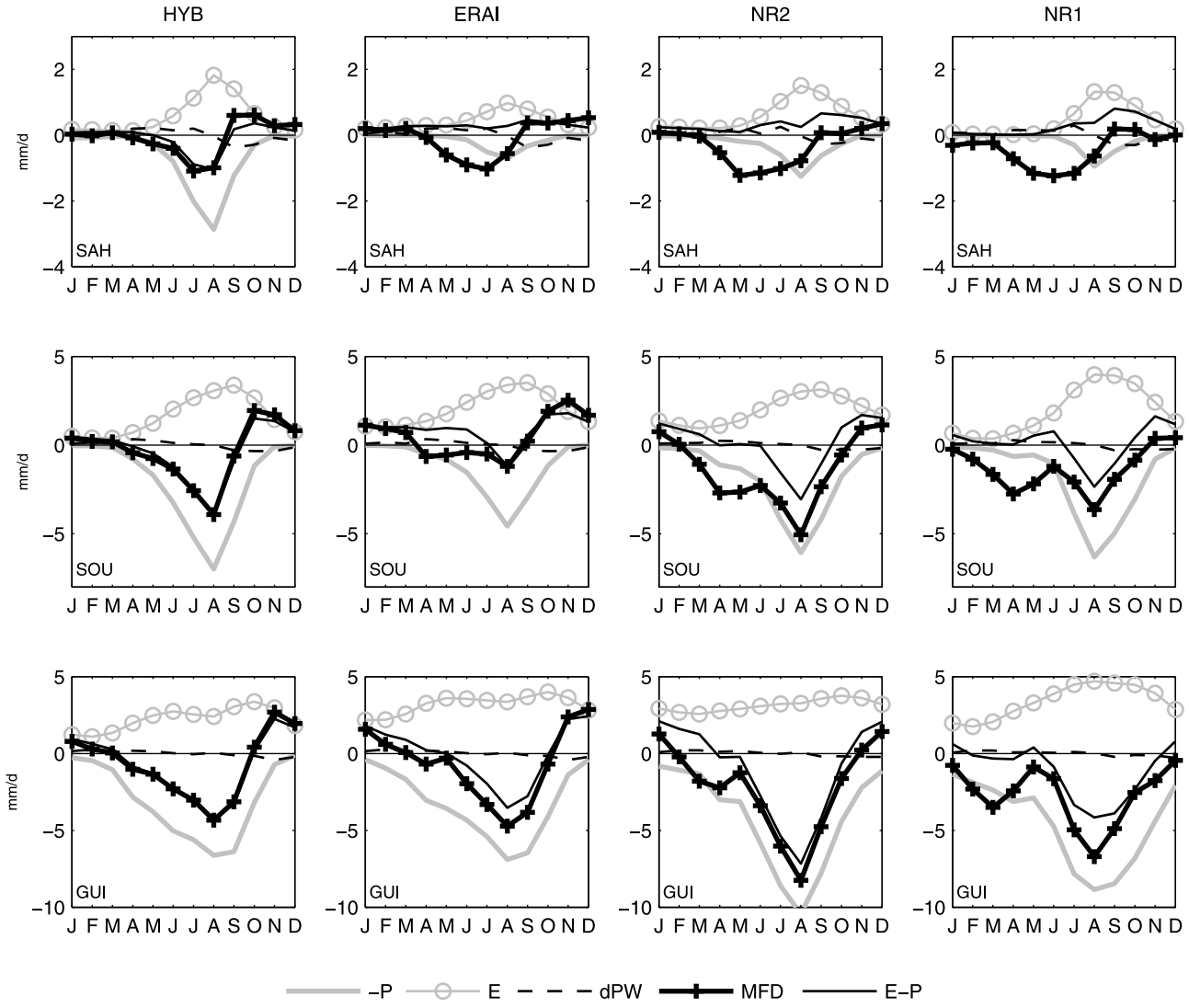

Figure 4. Monthly mean moisture budget terms for the same four data sets as those in Figure 2, averaged in the SAH, SOU, and GUI boxes over years 2002–2007. Units are mm d^{-1}.

fundamental difference is obviously due to the nature of the data (AN versus FC variables). In the SAH box, all three reanalyses show an excess of moisture flux convergence in May and June (especially NCEP reanalyses) but this is not associated with an excess of rainfall or an increase of the humidity storage in the models. It thus produces an imbalanced water budget in the reanalyses (see also Figure 5). Later, in July–September, the reanalyses show MFD_{AN} values consistent with MFD_{hyb} but again the relationship with P_{FC} is poor and largely in deficit then. In the SOU box, the NCEP reanalyses show an excess of moisture flux convergence in April–May, similar to what is observed in May–June in the SAH box. More generally, the NCEP reanalyses overestimate moisture flux convergence all year long and show a minimum in June that is not seen in MFD_{hyb}. ERA-Interim shows small values of moisture flux convergence, especially in June–September when it is related to the large spatial pattern of moisture divergence previously discussed (Figure 3). On the other hand, the NCEP reanalyses do not represent well the moisture divergence during the dry season. In the GUI box, ERA-Interim represents quite well the seasonal evolution of MFD (both in phase and amplitude), whereas the NCEP reanalyses show the same deficiencies as in the SOU box, except for an increased bias in MFD_{AN} in August (around 4 mm d^{-1}). The excess in MFD_{AN} in both NCEP reanalyses might be linked to their excess in precipitation.

3.3. Budget Closure Issues

[30] A large residual was diagnosed in Table 2 ($E_{FC} - P_{FC} > MFD_{AN}$ with $dPW_{AN} \sim 0$) in the three reanalyses and in all three boxes, consistently with past studies [*Kanamitsu and Saha*, 1996; *Roads*, 2003; *Trenberth and Guillemot*, 1995]. The seasonal evolution of this residual is shown as Res_a in Figure 5a. It is negative almost all year long and its magnitude can be as large as the individual budget terms. According to equation (5), a negative residual is a result of one or several of the following inconsistencies in the reanalyses: too strong evapotranspiration (E_{FC}), too weak precipitation (P_{FC}) and/or a too strong moisture flux convergence (MFD_{AN}). In the SAH box, all three factors act

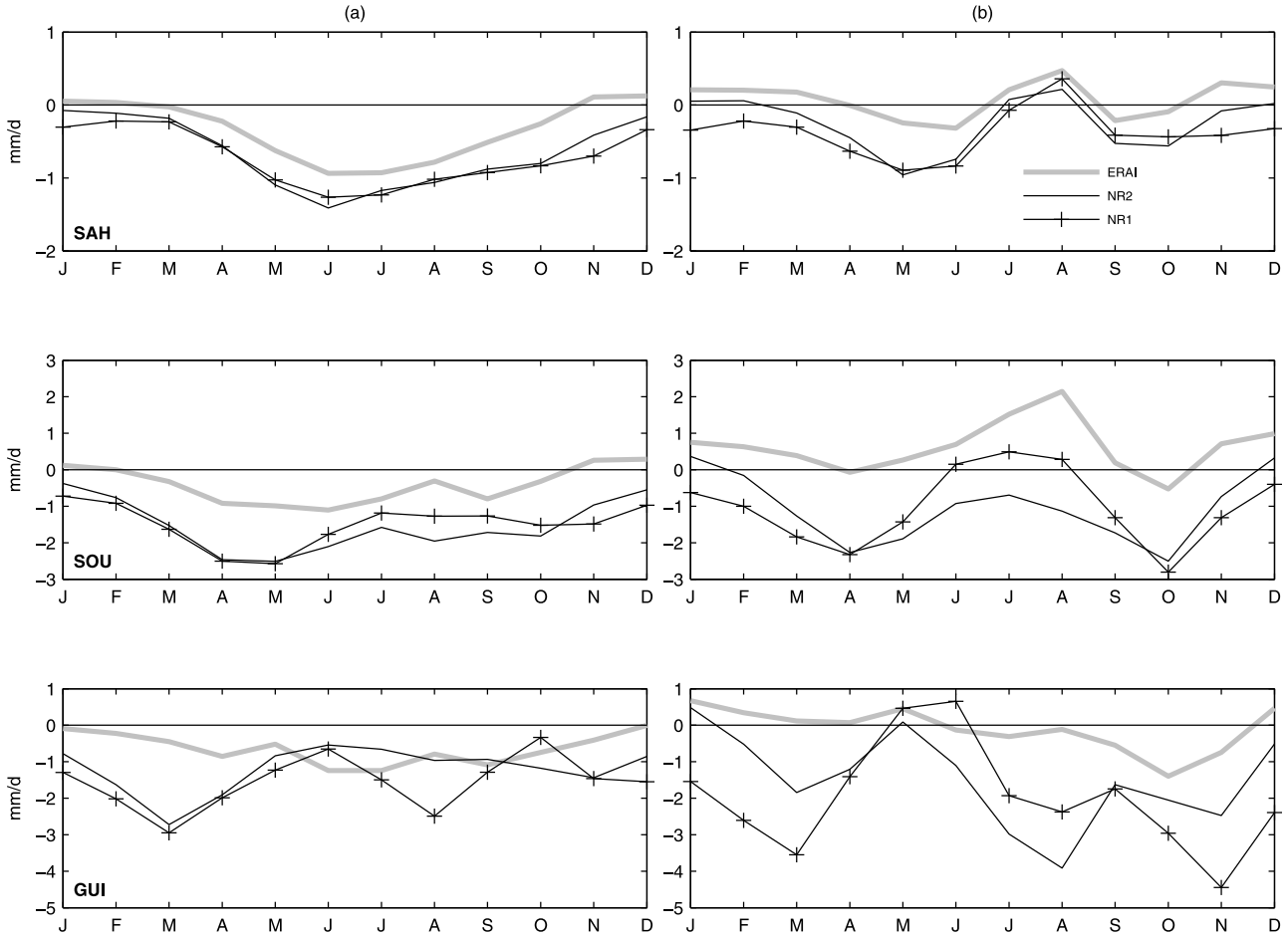

Figure 5. Water budget residuals from two data sets: (a) mixing of analysis (AN) and forecast (FC) terms from numerical weather prediction (NWP) systems, $\mathrm{Res}_a = \mathrm{MFD_{AN}} + \mathrm{dPW_{AN}} - (E_{\mathrm{FC}} - P_{\mathrm{FC}})$, and (b) mixing of AN terms from NWP systems and the hybrid data set, $\mathrm{Res}_b = \mathrm{MFD_{AN}} + \mathrm{dPW_{AN}} - (E_{\mathrm{ALMIP}} - P_{\mathrm{TRMM}})$. Units are mm d^{-1}.

simultaneously. In the SOU box, the residual shows a large peak (~2 mm d^{-1} in the NCEP reanalyses), between April and June, prior to the monsoon onset. In this box, ERA-Interim shows the smallest residuals all year long, but this hides large compensating errors in the individual terms. Indeed, $\mathrm{MFD_{AN}} \approx E_{\mathrm{FC}} - P_{\mathrm{FC}}$ but $\mathrm{MFD_{AN}}$ is significantly biased compared to $\mathrm{MFD_{hyb}}$ (see Figure 4 and Res_b in Figure 5b). In the GUI box also, the smallest Res_a residuals are found in ERA-Interim, but there, the individual terms are close to the hybrid estimates (only E_{FC} is slightly biased; Figure 4). The NCEP reanalyses exhibit again large residuals, up to $\mathrm{Res}_a = -3$ mm d^{-1} in March due to an excess of moisture flux convergence (Figure 4) and −2 mm d^{-1} in August due to an excess of rainfall (especially in NCEP-R2). On the basis of investigations with ECMWF-IFS model (see the Appendix A), the large negative residuals are believed to reflect the presence of analysis increments and to a lesser extent computational errors in $\mathrm{MFD_{AN}}$ (see the two last columns of Table A1).

[31] Since E_{FC}, P_{FC}, and $E_{\mathrm{FC}} - P_{\mathrm{FC}}$ from the reanalyses contain significant biases and the budget is not balanced with their $\mathrm{MFD_{AN}} + \mathrm{dPW_{AN}}$ counterparts, the balance between $\mathrm{MFD_{AN}} + \mathrm{dPW_{AN}}$ and $E_{\mathrm{ALMIP}} - P_{\mathrm{TRMM}}$ is examined here (Figure 5b). The large negative residuals in the reanalysis budget (Res_a) are reduced and replaced in some instances by positive residuals (Res_b). For ERA-Interim, the closure is usually improved in the SAH and GUI boxes, but it worsens in the SOU box. For the NCEP reanalyses, the residual is generally not improved. Hence, the combination of $\mathrm{MFD_{AN}}$ and $\mathrm{dPW_{AN}}$ terms from reanalyses and E_{ALMIP} and $\mathrm{P_{TRMM}}$ from the hybrid data set is not really consistent either. Instead, this residual suggests that the analysis increments diagnosed above contribute significantly to the errors in the analyzed terms.

3.4. Interannual Variability

[32] Potentially, NWP reanalyses can provide water budget terms over long periods of time (up to 50 years) allowing the investigation of interannual variability [*Fontaine et al.*, 2003]. Here, we address their ability to reproduce the results obtained from the hybrid data set over 2002–2007 in part 1 of this study, with a focus on the monthly anomalies of P, E, and MFD.

[33] Table 2 reports the standard deviation of these anomalies together with linear correlation coefficients between the NWP estimates and the hybrid estimates.

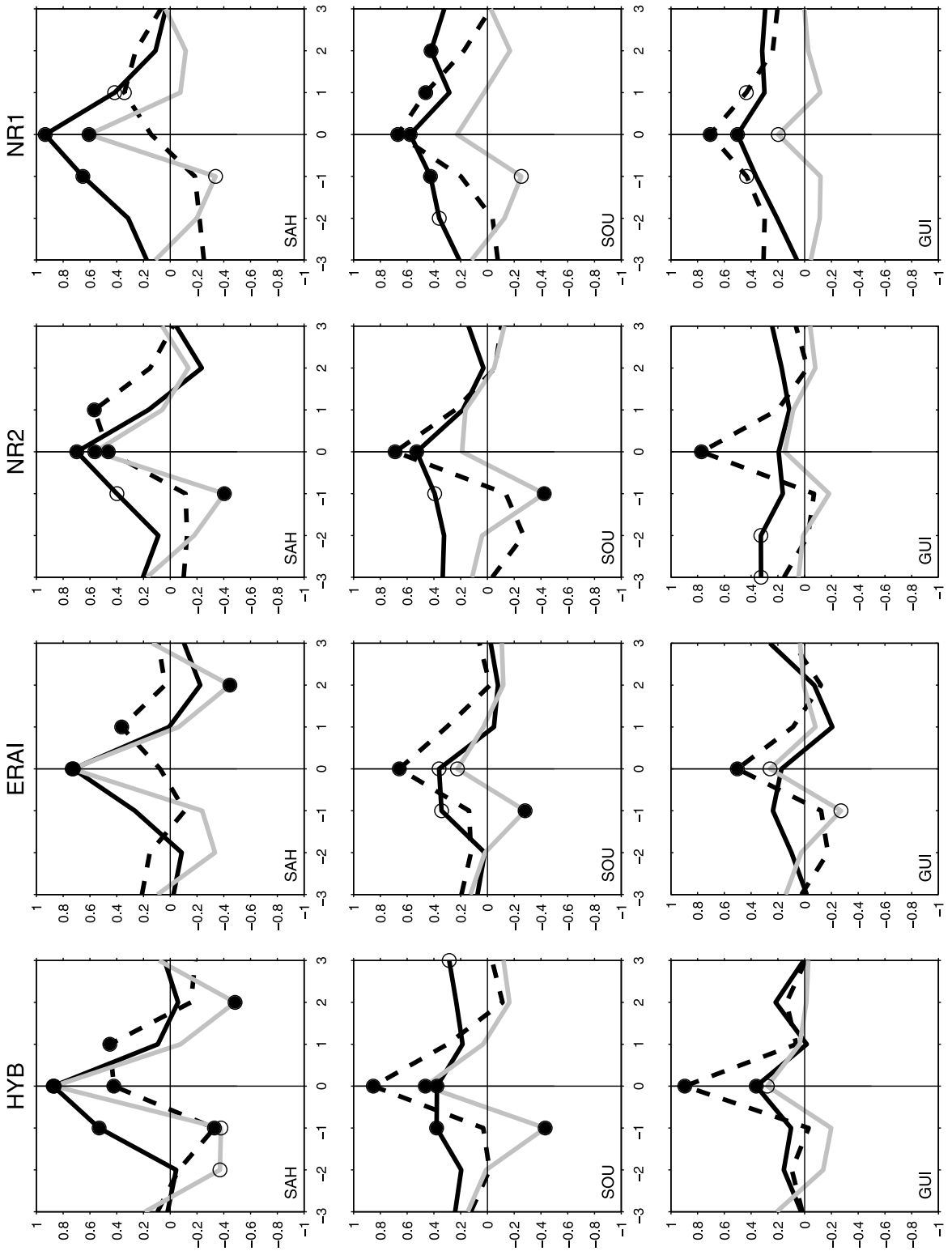

Figure 6. Lagged correlation functions of monthly mean anomalies of water budget terms for the same four data sets and boxes and in Figure 4. A negative lag means that the first variable leads the second one. The filled (open) circles are significant at the two-sided 0.01 (0.05) level according to a random-phase test [*Ebisuzaki*, 1997].

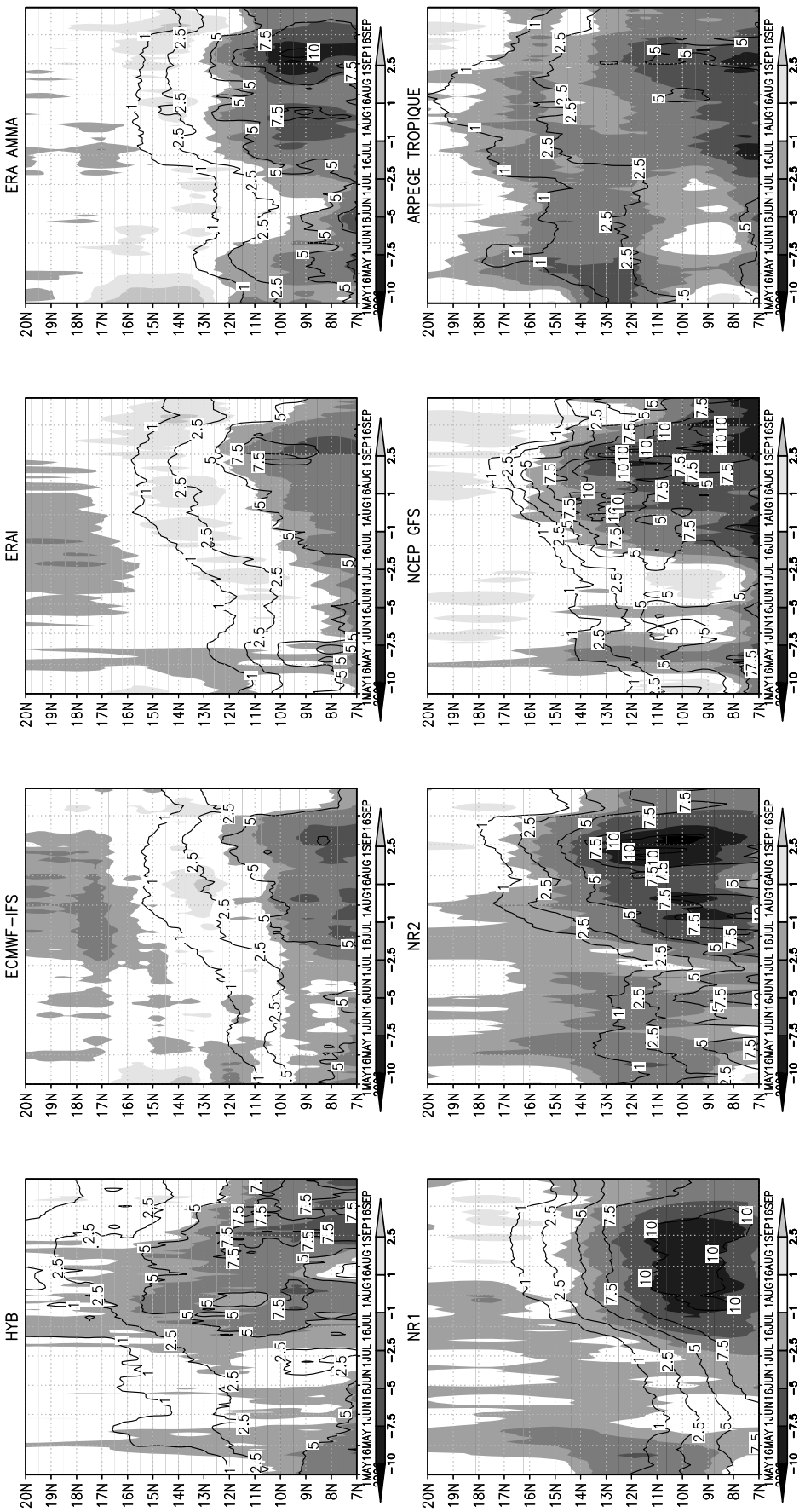

Figure 7. Time-latitude diagrams of moisture flux convergence (shaded) and precipitation (contours) averaged over 10°W–10°E for the period from May to September 2006. A 15 day running mean is applied. Units are mm d^{-1}.

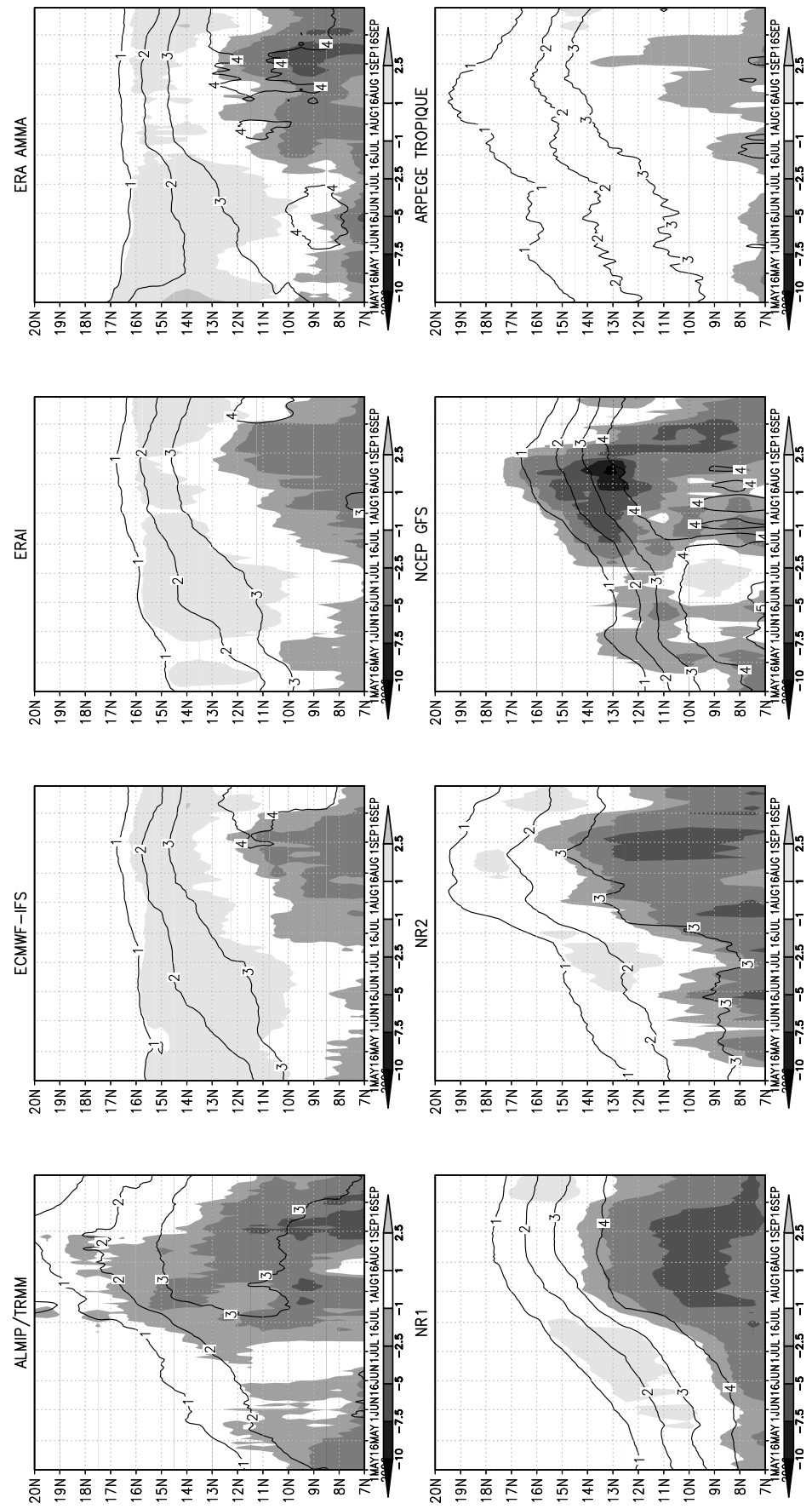

Figure 8. Similar to Figure 7, but for evapotranspiration minus precipitation (shaded) and evapotranspiration (contours).

Overall, ERA-Interim and NCEP-R2 perform fairly well in all three boxes, while NCEP-R1 shows overall poor correlations with the hybrid budget terms. For the three reanalyses, the highest correlations are obtained in the SAH box, followed by the SOU box and then the GUI box. In terms of variance, ERA-Interim shows too weak fluctuations in ΔP in all three boxes, while it is the opposite for NCEP-R2, and too weak variance in ΔE, while NCEP-R2 shows good results (consistent with Figure 4). The variance and correlation in ΔMFD are the best for ERA-Interim, at least in the SOU and SAH boxes. In the GUI box, the correlation in ΔMFD is the best for NCEP-R2. Hence, ERA-Interim and NCEP-R2 appear to capture some features of the interannual variability of the water cycle. A similar analysis based on annual mean quantities (for 6 years only) yields poor results with no statistical significance (not shown).

[34] Figure 6 shows cross-correlation functions of monthly anomalies. This is a useful tool for understanding causality between water budget terms. The most significant correlations are (1) between ΔP and ΔE in the SAH box, at lags 0 and −1 month, meaning that the occurrence of a maximum in ΔE is following a maximum in ΔP with a delay of 0–1 month; (2) between –ΔMFD and ΔdPW at lag 0 in the SAH box, reflecting the strength of humidity advection in the region of the ITD and its major role in fluctuations in water vapor amount; and (3) between ΔP and –ΔMFD at lag 0 in SOU and GUI boxes, and at lag 0 and +1 month in the SAH, implying that an increase in precipitation is associated with a simultaneous increase in convergence in the SOU and GUI boxes, while this increase in convergence starts ~1 month earlier in the SAH box.

[35] Overall, the reanalyses reproduce all the significant correlations seen with the hybrid data set, including the contrast between the SAH box and the two other boxes. However, the correlation coefficients are generally smaller in the reanalyses. Hence, it can be concluded that the reanalyses provide some insight into the interannual variability in water budget terms, at least at the monthly mean time scale, but the magnitude of the anomalies (Table 2) and the link between budget terms (Figure 6) remain of limited accuracy.

4. AMMA Reanalysis and Operational Analyses

4.1. Spatial and Temporal Evolution of Water Budget Terms During the SOP 2006

[36] The goal here is to examine more closely the spatiotemporal relationship between P and MFD and, at the same time, between E and P, for the period from May to September 2006 (the AMMA Special Observation Period (SOP) [*Lebel et al.*, 2009]), with an enhanced ensemble of the NWP systems. Therefore, operational analyses (ECMWF-IFS, NCEP-GFS, and ARPEGE-Tropiques) and the AMMA reanalysis (ERA-AMMA) are included. These models benefited from more recent models physics and higher spatial resolution compared the previous reanalyses (see Table 1) and from enhanced observations during the AMMA-SOP. The impact of these additional data on the ECMWF and ARPEGE analyses and forecasts was investigated in details by *Agustí-Panareda et al.* [2010] and *Faccani et al.* [2009], respectively.

[37] Figures 7 and 8 show time-latitude diagrams of MFD and P, and E-P and E, respectively. The hybrid data set is first analyzed as it is our reference. The P_{TRMM} = 1 mm d^{-1} limit is seen to migrate from 12°N to 20°N, between May and mid-July 2006. Large intraseasonal fluctuations are observed, with two northward excursions around 20 May and 15 June (preonset period) and one on 10 July, associated with the late monsoon onset in 2006 [*Janicot et al.*, 2008]. The E_{ALMIP} = 1 mm d^{-1} isoline is seen to move northward with a short time lag with respect to the P_{TRMM} = 1 mm d^{-1} rainfall isoline. In contrast, MFD_{hyb} reaches this level (−1 mm d^{-1}) only during the two northward rainfall excursions of 20 May and 10 July. More to the south, the P_{TRMM} = 2.5 mm d^{-1} limit shows similar but more regular northward excursions between May and September, while P_{TRMM} = 5 mm d^{-1} delimits roughly the core of the rainbelt and is associated with the monsoon jump between 5°N and 10°N [*Sultan and Janicot*, 2000]. The areas of larger rainfall are well correlated with larger evapotranspiration (with $P_{TRMM} > E_{ALMIP}$ most of time) and larger moisture convergence. MFD_{hyb} shows significant intraseasonal variability during the core of the season in the northern Sahel (15°N–20°N), from mid-July to September, but also a reduction to the south before the onset (7°N–11°N, 10 June to 10 July) consistent with reduced precipitation.

[38] Overall, none of the NWP systems reproduces satisfactorily this ensemble of features. All three ECMWF model versions show a too southerly P_{FC} = 1 mm d^{-1} limit (~15.5°N in August) and inconsistent $E_{FC} > P_{FC}$ in the Sahel. The rainfall limit extends slightly more to the north in ERA-Interim and ERA-AMMA compared to ECMWF-IFS. ERA-AMMA shows also stronger rainfall and larger moisture convergence more to the south, especially after the onset (e.g., P_{FC} = 5 mm d^{-1} limit reaching 12.5°N instead of 11°N in ECMWF-IFS) and reduced moisture convergence to the north, in the region of the ITD, compared to ERA-Interim and ECMWF-IFS. Hence, among the three ECMWF products, ERA-AMMA is the more realistic, though the rainbelt is still too much to the south. Note that in ERA-AMMA the high values of evaporation over Sahel during May are due to an error in the initialization of soil moisture which occurred during the run of the reanalysis experiment. This problem is corrected in a newer version of the reanalysis. A common deficiency in all three ECMWF products is the region of moisture divergence at 11°N–13°N in June and 13°N–15°N in August (consistent with the 6 year mean of ERA-Interim; Figure 3), which is suspected to act as a blocking zone for the rainbelt. It is also seen in the forecast version of MFD (Agustí-Panareda et al., submitted manuscript, 2009).

[39] The three NCEP model versions are very different. NCEP-R2 and NCEP-GFS show more realistic rainfall patterns than NCEP-R1 and ECMWF forecasts. The P_{FC} = 1 mm d^{-1} limit reaches its northernmost position at 17°N in August–September, which is improved but still too south compared to TRMM. Interestingly, in NCEP-GFS the P_{FC} = 5 mm d^{-1} limit reaches 16°N in August, but the meridional gradient to the north of this limit is too abrupt and rainfall is too strong between 10°N and 15°N. The evapotranspiration pattern in all three models is fairly correlated with precipitation, but only NCEP-GFS shows $E_{FC} < P_{FC}$ at the northern limit of the rainbelt in a way

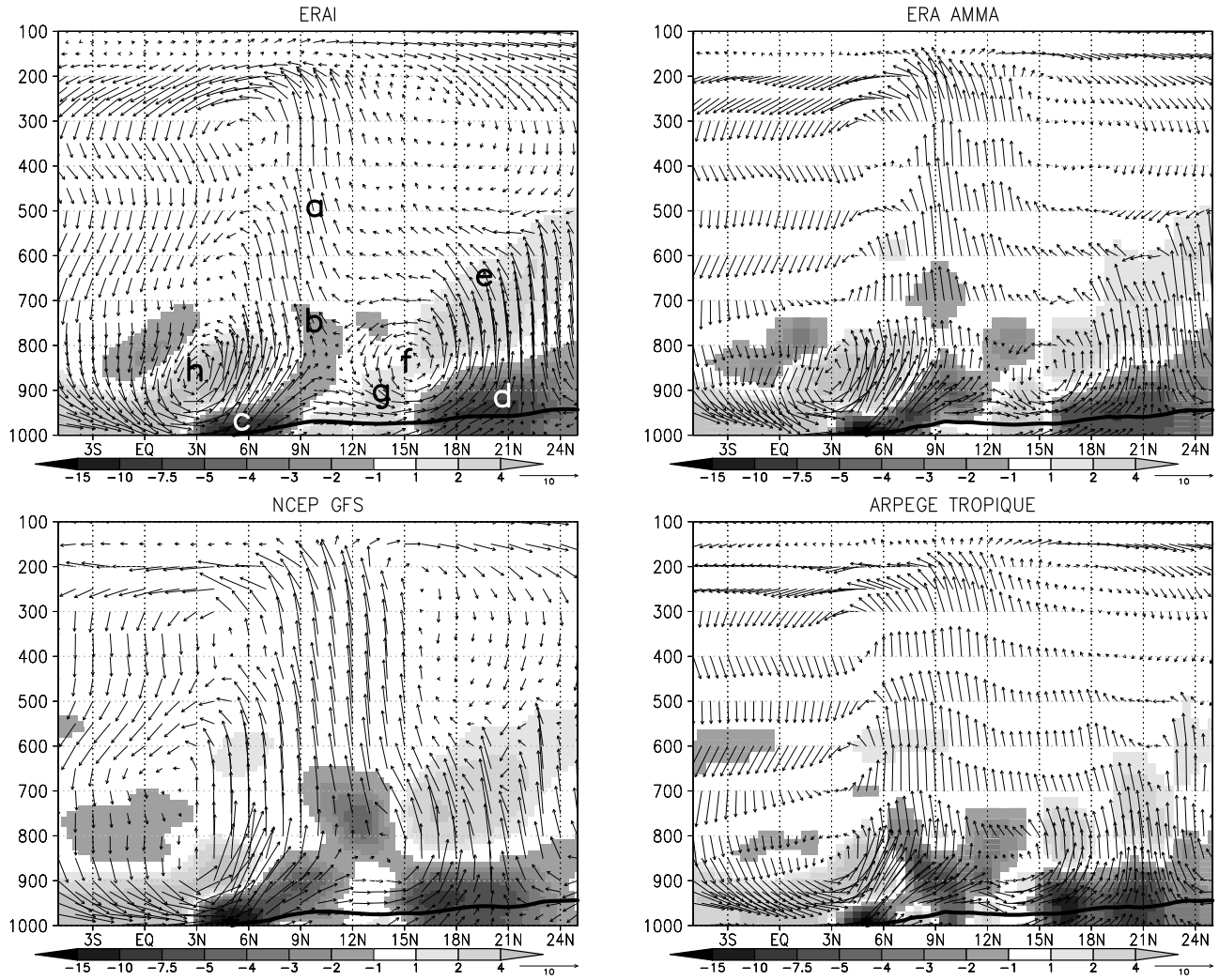

Figure 9. Vertical cross section of moisture flux convergence ($\times 10^8$ s^{-1}, shading) and meridional (m s^{-1}) vertical wind vectors (vertical scale $\times$ 100 Pa s^{-1}) averaged over 10°W–10°E for August 2006.

consistent with the hybrid data set. The onset is also better represented in NCEP-GFS, both in P_{FC} and MFD_{AN}. Overall, this model shows significant improvements over the older NCEP model versions, namely, a more satisfactory link between E_{FC} and P_{FC}, and between P_{FC} and MFD_{AN}. A distinct feature in this model compared to the others is the zone of moisture divergence located north of 16°N.

[40] ARPEGE-Tropiques, in contrast to the other models, simulates a quite realistic northward propagation of the rainbelt, with the P_{FC} = 1 mm d^{-1} limit reproducing the preonset excursions (20 May, 15 June, and 10 July) and reaching 19°N in August. However, precipitation is overall too weak and moisture flux convergence comparatively too large, especially to the north during the preonset period. The evapotranspiration pattern is also well correlated with precipitation but the balance between E_{FC} and P_{FC} is incorrect (the region where $E_{FC} \sim P_{FC}$ extends too much to the south). This suggests a sensitivity of the soil moisture analysis to other features of the model (e.g., surface and turbulence schemes), as this analysis system is similar to that of the ECMWF-IFS.

4.2. Atmospheric Circulation

[41] To better understand why the NWP analyses show such striking differences in MFD_{AN}, it is necessary to examine the vertical structure of MFD_{AN} and the atmospheric circulation. This is done only with ERA-Interim, ERA-AMMA, NCEP-GFS, and ARPEGE- Tropiques. Figure 9 presents the vertical cross section of MFD_{AN} and meridional-vertical wind vectors for August 2006. Figure 10 shows the three wind components separately. All four analyses provide a qualitatively similar picture of the mean circulation. Specific features are indicated for ERA-Interim (small letters superimposed on the plot in Figure 9). These features are as follows: (1) a zone of deep convection (usually referred to as the Intertropical Convergence Zone (ITCZ)) extending from 800 to 200 hPa and centered at 10°N, which corresponds to the ascending branch of the Hadley cell, the subsidence branches being located to the south (3°S) and to the north (22°N); (2) a band of moisture flux convergence beneath the northern flank of the ITCZ (1000–700 hPa, 10°N); (3) a zone of shallow convection and strong moisture flux convergence near the coast (1000–

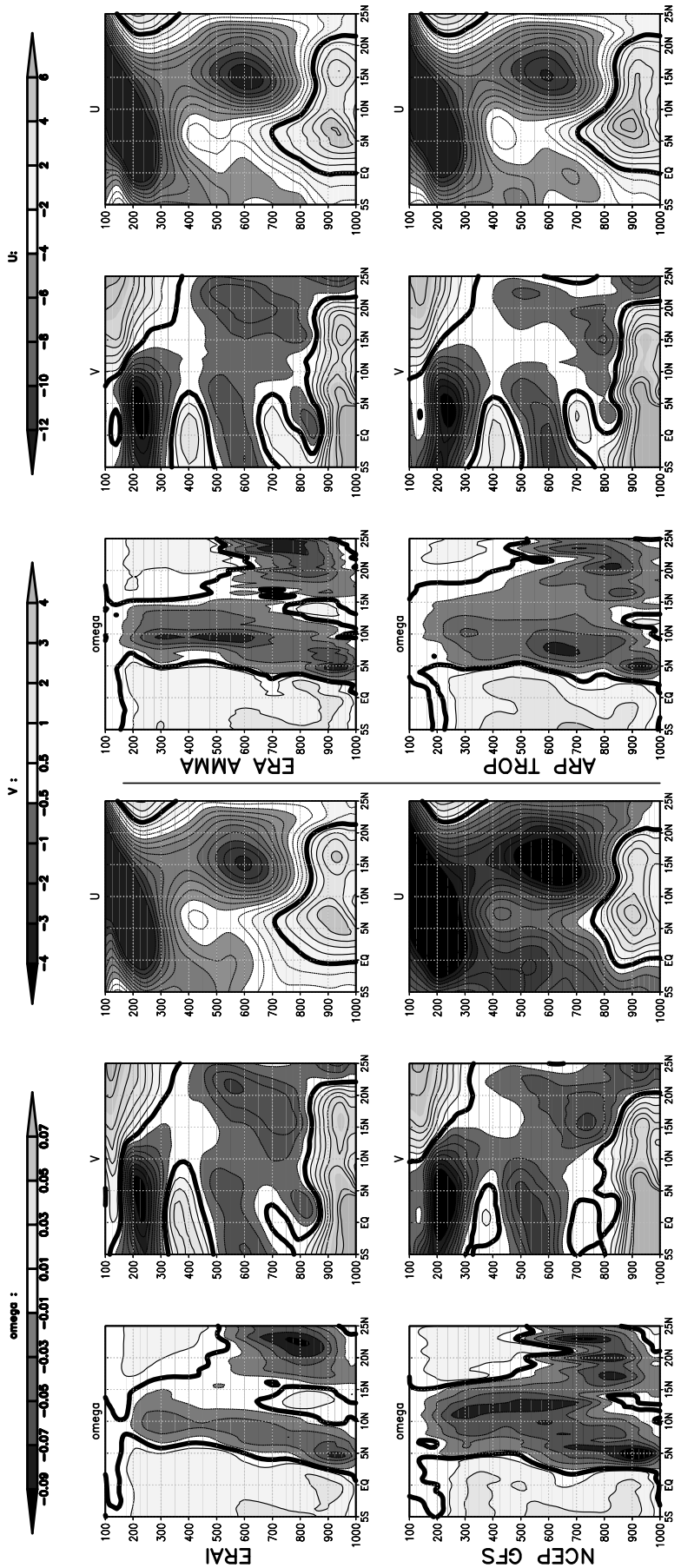

Figure 10. Vertical cross section of wind vector components averaged over 10°W–10°E for August 2006: (left) vertical (Pa s^{-1}), (middle) meridional (m s^{-1}), and (right) zonal (m s^{-1}).

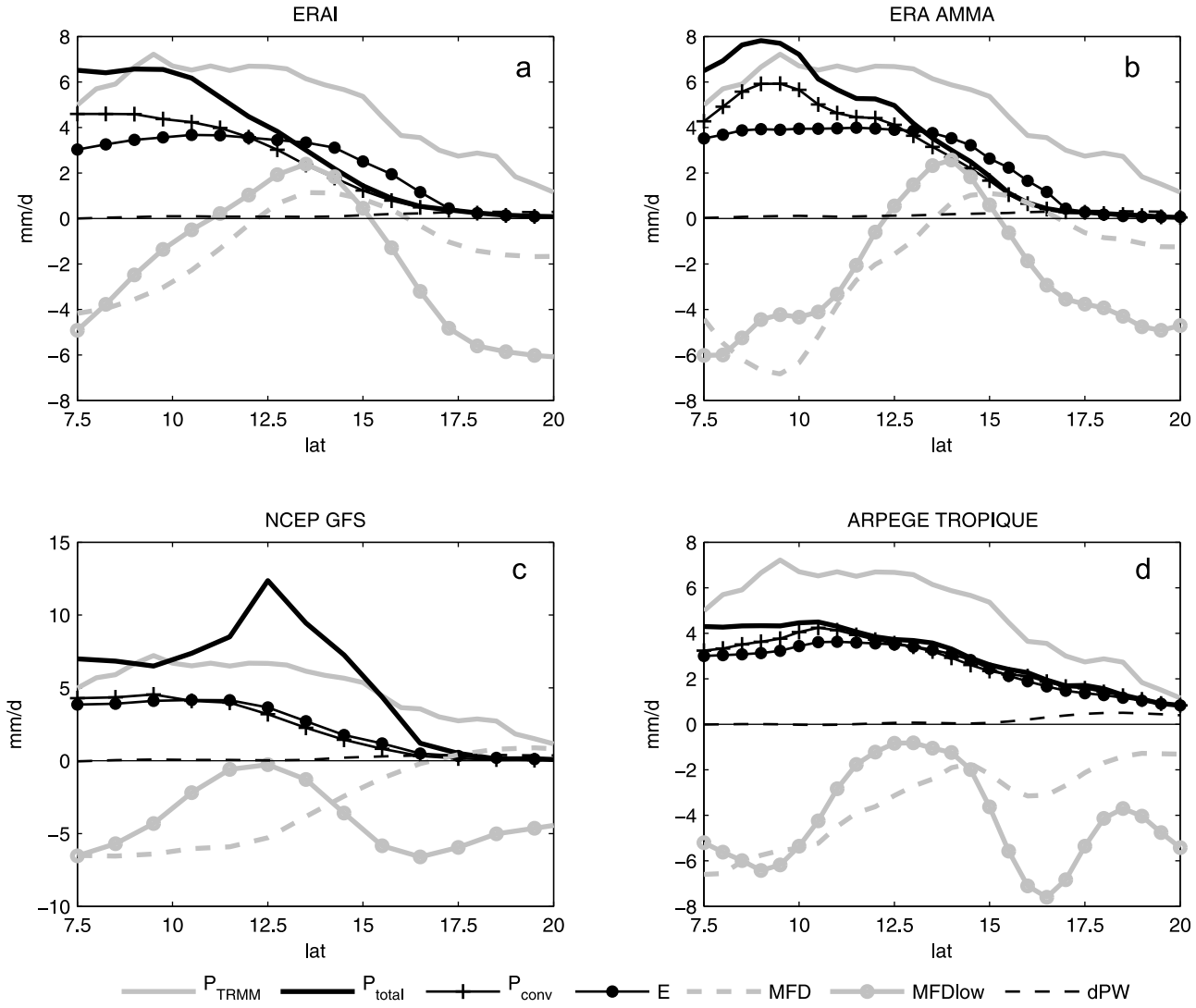

Figure 11. Latitudinal cross section of TRMM precipitation (P_{TRMM}), total precipitation (P_{total}), convective precipitation (P_{conv}), and evapotranspiration (E) from NWP model simulations, total moisture flux divergence (MFD), low-level moisture flux divergence (MFD_{low}, integrated from the surface to 850 hPa), and precipitable water tendency (dPW) from NWP model analyses: (a) ERA-Interim, (b) ERA-AMMA, (c) NCEP Global Forecasting System (GFS), and (d) ARPEGE-Tropiques. The data are averaged over 10°W–10°E for August 2006. Units are mm d^{-1}.

925 hPa, 3°N–8°N); (4) strong low-level moisture flux convergence to the north (1000–850 hPa, 16°N–25°N) in the region of the ITD and the heat low, which drives strong vertical motion up to 600 hPa at 21°N; (5) a layer of moisture divergence (800–550 hPa, 16°N–25°N) capping the previous low-level moisture convergence layer; (6) a northerly shallow meridional circulation (SMC) between the ITCZ and the ITD, with its vortex located at 850 hPa, 15°N, associated with the strong vertical motion in the region of the heat low, the southerly low-level monsoon flow (1000–900 hPa), and the northeasterly flow overriding the southwesterly monsoon flow (800–500 hPa); (7) a region of low-level moisture divergence between the ITCZ and the ITD (1000–850 hPa, 10°N–15°N) associated with the subsiding branch of the northerly SMC; and (8) a southerly SMC at 850 hPa, 3°N, embedded in the southerly Hadley cell, associated with the low-level southerly monsoon flow and a layer of northerly return flow at 800 hPa. Figure 10 more clearly shows that the latter is the lowest of three layers with a northerly component in the main flow south of the ITCZ, the other two being at the levels of the AEJ (600 hPa) and the TEJ (200 hPa).

[42] While nearly all the analyses represent the features listed above, the intensity and location of circulation and MFD_{AN} patterns differ substantially among them. A major difference can be seen in the northerly SMC (Figure 9f). In the ECMWF reanalyses, the overturning circulation of this SMC is especially strong and appears as a major explanation of the strong moisture divergence taking place in the low levels (Figure 9g). The subsiding branch of this SMC is associated with advection of dry air from the Saharan air layer. In the NCEP-GFS and ARPEGE-Tropiques analyses, the SMC and subsiding branch are present as well, but they are much weaker (this is the case also for NCEP-R1 and

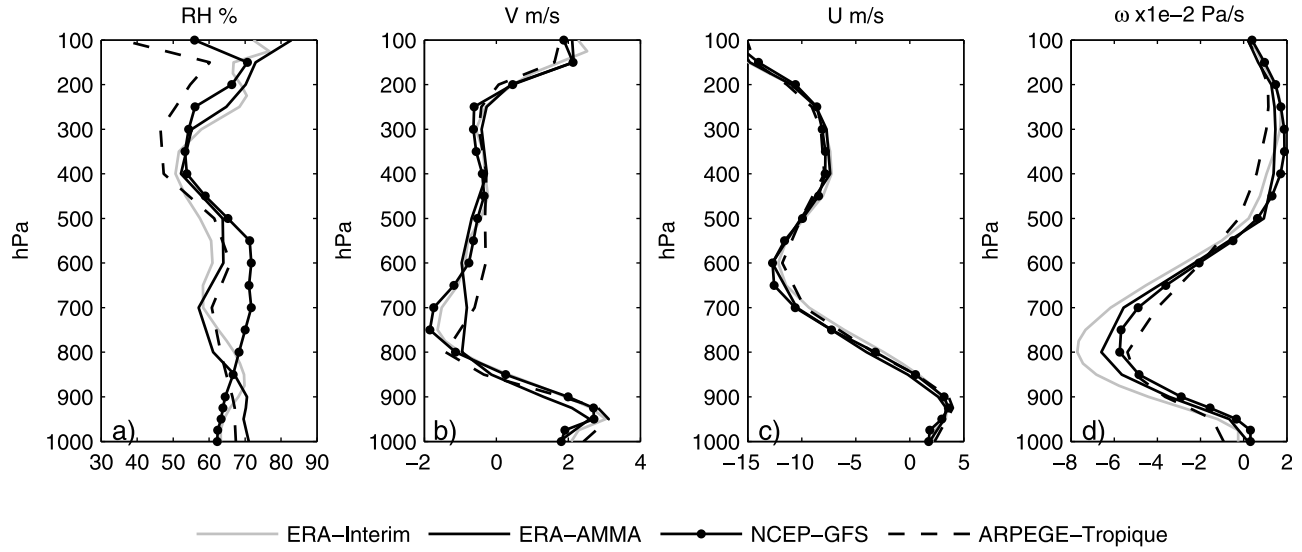

Figure 12. Vertical profiles of (a) relative humidity (%), (b) meridional and (c) zonal (m s^{-1}) wind components, and (d) vertical velocity (Pa s^{-1}) for NWP model analyses: ERA-Interim (shaded line), ERA-AMMA (solid line), NCEP-GFS (dotted line), and ARPEGE-Tropiques (dashed line). Data in Figures 12a–12c are averaged over the low-level subsiding zone (10°W–10°E × 13°N–16°N; see Figure 10), and Figure 12d is averaged over the heat low region (10°W–10°E × 20°N–25°N; see Figure 9d) for August 2006.

NCEP-R2; not shown). As a result, the zone of low-level moisture divergence (Figure 9g) is much smaller and weaker in these analyses and their vertically integrated MFD_{AN} (Figure 7) is dominated by moisture convergence at the northern flank of the ITCZ (10°N–15°N). Similar reasoning explains also the difference in vertically integrated MFD_{AN} in the region of the ITD (15°N–25°N): some analyses show stronger low-level moisture convergence and others stronger midlevel moisture divergence (e.g., NCEP-GFS).

[43] As discussed above, the northerly SMC (Figure 9f) is driven by three main components. In the ECMWF analyses, all three components are stronger (Figure 10), but especially the southwesterly monsoon flow. Indeed, this model shows a secondary maximum in the low-level flow around 17°N, 925 hPa, with an acceleration of the flow between 10°N and 17°N. This acceleration is consistent with the strong subsidence seen at 850 hPa, 13.5°. Inspection of radiosonde profiles at Niamey and Tombouctou confirms the too strong southerly flow at 925 hPa and too strong northerly flow above 800 hPa in the ECMWF analyses (not shown). *Zhang et al.* [2008] also noticed a difference in the northerly flow component of the SMC in the previous ECMWF reanalysis (ERA40) and the NCEP reanalyses, which they attributed to differences in the parameterization of cumulus convection. However, other physical components of the model could well play a role, such as surface and turbulent processes, as well as cloud and aerosols radiative effects.

4.3. Interactions Between Atmospheric Circulation, Precipitation, and Moist Processes

[44] Figure 11 highlights the main features of the West African Monsoon water budget and the deficiencies in four of the NWP systems. In the ECMWF reanalyses, the bias in precipitation appears as an abrupt decrease in rainfall between 10°N and 15°N, as compared to P_{TRMM}. This strong gradient coincides with a zone of strong moisture divergence, originating in the low levels, between 12°N and 15°N. It is very likely that the divergence blocks convection and prevents further northward migration of the rainbelt. Indeed, precipitation in this region is mostly of convective nature and the convection parameterization in this model is dependent on CAPE and atmospheric humidity [*Bechtold et al.*, 2008] which both are linked to low-level moisture convergence. The excess of E_{FC} over P_{FC} in the two ECMWF reanalyses may further participate to enhance moisture flux divergence in the atmospheric column ($MFD_{AN} > 0$ where $E_{FC} > P_{FC}$). In NCEP-GFS and ARPEGE-Tropiques, a drop in precipitation is observed as well north of 12.5°N, along with a strong decrease in moisture convergence but the latter does not turn into divergence. In ARPEGE-Tropiques, the latitudinal decrease in precipitation is smoother than in the other models and the rainbelt is extending more to the north but the amount of simulated rain is nevertheless too weak. In NCEP-GFS, total precipitation is largely overestimated in the region 10°N–16°N. This is due to an excessive amount of large-scale precipitation in this model. But convective precipitation in NCEP-GFS is consistent with the other models. Similar problems have been observed previously with this model over the USA and are explained as an artifact of the convective scheme referred to as grid-scale convection (http://www.hpc.ncep.noaa.gov/qpfbombs/). The excess of large-scale precipitation is associated with too moist midlevels in NCEP-GFS over West Africa (Figure 12a). This problem is not seen in the NCEP reanalyses (not shown).

[45] The role of the northerly SMC around 15°N is further investigated with Figure 12. Interestingly, the northerly flow is seen to extend through a large part of the troposphere (850–200 hPa). It is thus advecting dry air from the Sahara in the middle and upper levels which enhances convective inhibition and evaporation of falling rainfall. It can be

hypothesized that this feature adds to the blocking of convection and bias of precipitation in the Sahel. In the ECMWF reanalyses, an excessively strong vertical motion in the heat low (800 hPa; Figure 12d) appears as a major explanation for strong overturning circulation associated with the SMC (700–800 hPa; Figure 12b). The origin of the too strong heat low seems to be linked with a large underestimation of the aerosol content in the Sahara in the ECMWF model leading to a large overestimation of surface incoming radiation [*Guichard et al.*, 2010; Agustí-Panareda et al., submitted manuscript, 2009]. Very likely, other factors are involved too, such as the surface albedo, vegetation and roughness length which are prescribed in the ECMWF model. Indeed, the latitudinal extent of the rainband is expected to be sensitive to the choice of surface albedo and aerosol amounts [*Peyrillé et al.*, 2007]. In addition, the feedback from vegetation onto the atmosphere along the seasonal cycle is not well represented in such models. Recent improvements in the parameterized physics [*Bechtold et al.*, 2008] and correction of dry bias in radiosonde observations [*Agustí-Panareda et al.*, 2009] have demonstrated a positive impact in ERA-AMMA. The strength of the heat low circulation (Figure 12d) is reduced in this reanalysis, as well as the meridional wind in the monsoon flow at 925 hPa and in the return flow at 750 hPa (Figure 12b). The rainbelt extends slightly further north and the low-level divergence at 13°N–16°N is reduced (Figure 11). Also, the low (925 hPa) and middle (600 hPa) levels are moister (Figure 12a). Further improvements of this model are expected with the introduction of interactive aerosols and land surface schemes (Agustí-Panareda et al., submitted manuscript, 2009).

5. Summary and Conclusion

[46] The confrontation of water budget terms from NWP reanalyses over West Africa to the reference hybrid data set presented in part 1 of this study [*Meynadier et al.*, 2010] has highlighted several similar deficiencies in the NWP systems which suggest similar origins. The deficiencies imply the representation of moist processes, the radiation budget, soil moisture analysis, and errors in radiosonde humidity observations. This study has also highlighted the critical role played by atmospheric circulation features specific to West Africa in shaping the seasonal evolution of the water cycle: the moist southwesterly monsoon flow, the shallow meridional circulation (SMC) connected with the heat low and the associated dry northerly return flow at 700 hPa, and convergence in the ITD region. All these features are strongly coupled and small misrepresentations associated with the above mentioned deficiencies in the NWP systems result in large biases in the atmospheric water and energy budgets.

[47] The central problem diagnosed in most of the NWP models is a too steep meridional gradient in simulated precipitation, with too large cumulated values south of 10°N (up to 500 mm) and too small values north of 15°N (up to -250 mm). This bias turns into a too southerly location of the rainbelt in the NWP models over West Africa. It suggests a deficiency in convective parameterizations and excessive convection inhibition possibly associated with a low-level subsidence to the north of the ITCZ (descending branch of the northerly SMC) and too large vertical mixing between the boundary layer and the deep layer of northerly dry air advected at midlevels (800–400 hPa) The SMC appears too strong in some of the models (especially in the ECMWF model). It seems that this is a consequence of a too strong heat low due to biases in the radiative budget over the Sahel-Sahara associated to limitations in the way aerosols and land surface properties are treated there. It is also hypothesized that there is a positive feedback between the lack of clouds and precipitation in the Sahel and the excess of surface incoming radiation driving a too strong heat low circulation.

[48] Another large bias in the water budget of most of the NWP systems is found in the simulation of evapotranspiration. Similar to the bias in precipitation, a too steep meridional gradient is diagnosed. However, E_{FC} and P_{FC} appear rather poorly coupled in these NWP systems and a great variety of seasonal evolutions in evapotranspiration is found. The documentation of the NWP systems and the presence of large soil moisture increments in the ECMWF model (A. Agustí-Panareda et al., Impact of improved soil moisture on the ECMWF precipitation forecast in West Africa, submitted to *Geophysical Research Letters*, 2009) suggest that the soil moisture analysis methods should be improved. However, a better coupling of E_{FC} and P_{FC} in the models requires also that the bias in precipitation is reduced.

[49] Because of these biases, the annual surface water budget in the Soudano-Sahelian region (10°N–20°N) appears positive in these NWP systems ($E_{FC} - P_{FC} > 0$) whereas *Nicholson et al.* [1997] and *Meynadier et al.* [2010] reported a more physically sound negative *E-P* budget. A few other past studies agree with the latter two (at least on the sign of *E-P*) but only in the 5°N–15°N region [*Gong and Eltahir*, 1996; *Roads et al.*, 2002; *Fontaine et al.*, 2003]. North of 15°N, most of the past studies using NWP products were limited by the large biases in E_{FC} and P_{FC}.

[50] Another approach for investigating the surface water budget is through its atmospheric components, dPW and MFD [*Trenberth and Guillemot*, 1995]. However, the present study evidenced large closure errors (1–2 mm d^{-1}) both in the reanalyses and in the operational NWP systems, such that the equivalence between $E_{FC} - P_{FC}$ and $dPW_{AN} + MFD_{AN}$ is generally not satisfied and the accuracy of the dPW_{AN} and MFD_{AN} estimates can be questioned. A major problem in this approach is that mixing simulated terms, E_{FC} and P_{FC}, and analyzed terms, dPW_{AN} and MFD_{AN}, introduces analysis increments and numerical errors. The latter result from that fact that MFD_{AN} is computed directly from 6 hourly, instantaneous, gridded wind and humidity fields. They are estimated with ECMWF-IFS to be on the order of ~0.5 mm d^{-1} (bias and standard deviation) and to increase slightly in the vicinity of the ITD (all the NWP models overestimate moisture convergence there). Since the numerical errors are rather small, most of the water budget closure error must result from analysis increments. The investigation with ECMWF-IFS revealed that the increments stem almost equally from dPW and MFD. The increment in dPW is mainly due to a drift in the short-term forecast as compared to independent GPS observations. This result is consistent with past studies using other NWP systems [*Higgins et al.*, 1996; *Trenberth and Guillemot*, 1998; *Bock et al.*, 2008]. The increment in MFD is obviously linked to the deficiencies evidenced above (in the moist processes, the radiation budget, the soil moisture analysis, and biases in radiosonde humidity observations). The

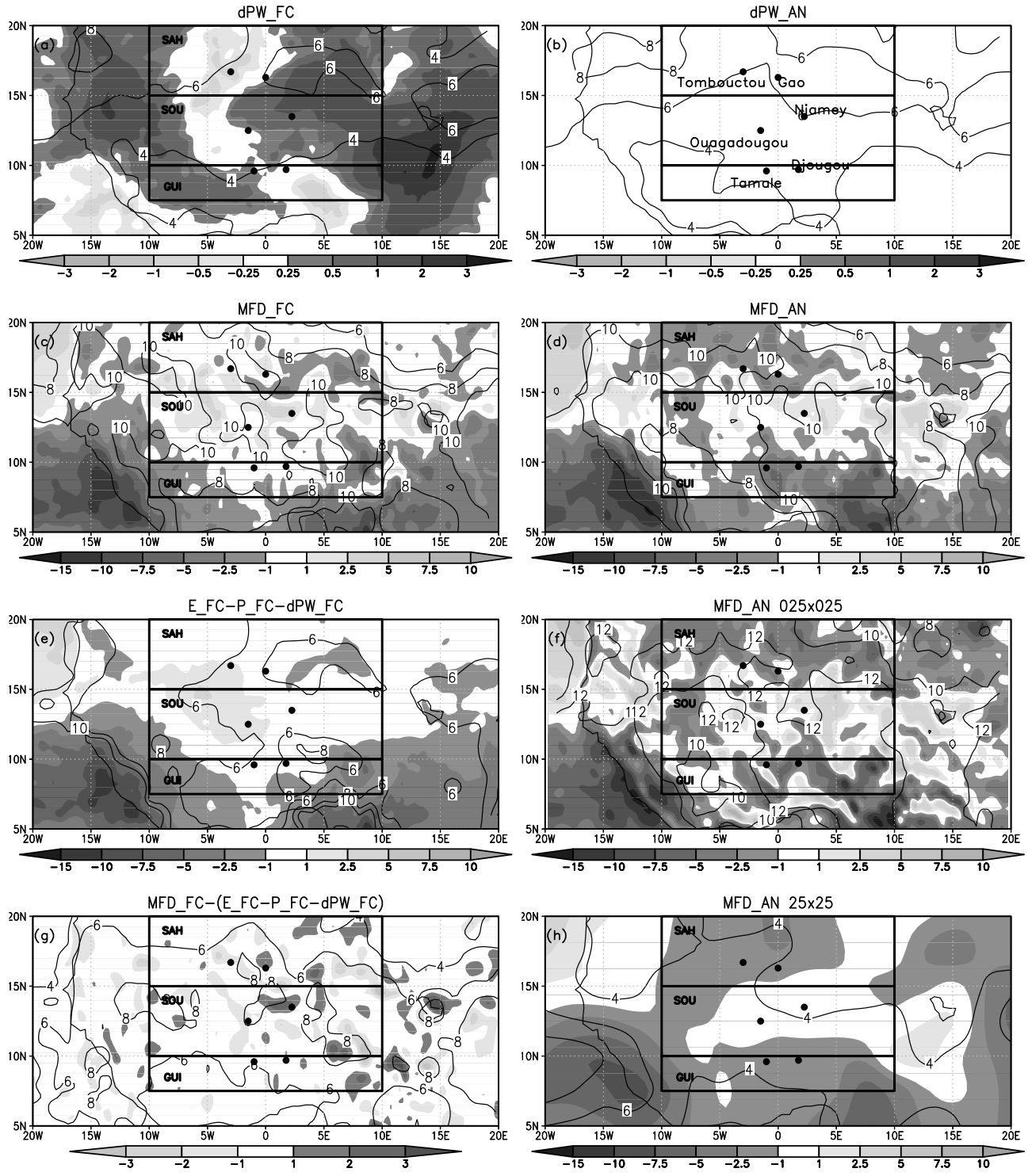

Figure A1. Water budget terms computed from (left) ECMWF Integrated Forecasting System forecasts (FC) and (right) analyses (AN): (a, b) dPW; (c, d) MFD computed from equation (1) on full model levels and 0.25° × 0.25° horizontal resolution, (e) MFD computed as residual from equation (2) $MFD_{FC,cumul} = E_{FC} - P_{FC} - dPW_{FC}$, (f) MFD_{AN} computed from pressure level data at 0.25° × 0.25° horizontal resolution. (g) FC budget closure error $Res_{FC} = MFD_{FC} - MFD_{FC,cumul}$, and (h) MFD_{AN} computed from pressure level data at 2.5° × 2.5° horizontal resolution. The shadings show quantities averaged over May–September 2006, and the contours show the standard deviation of daily quantities. Units are mm d^{-1}.

Table A1. Statistics of Water Budget Terms Computed From ECMWF-IFS Forecast (FC) and Analysis (AN), on Average Over the Period May–September 2006 and Over the Three Boxes Indicated in Figure 1[a]

Box	dPW_{FC}	dPW_{AN}	MFD_{FC}	MFD_{AN}	E_{FC}	P_{FC}	$MFD_{FC,cumul}$	Res_{FC}	Res_{AN}
SAH	0.49	0.09	−0.23	−0.96	0.55	0.16	−0.10	−0.14	−1.26
SOU	0.65	0.07	0.04	−0.30	2.98	2.13	0.20	−0.16	−1.08
GUI	0.39	0.01	−1.38	−2.65	3.76	4.98	−1.61	0.23	−1.42

[a]See caption of Figure A1. Units are mm d^{-1}. Abbreviations are as follows: AN, analysis; FC, forecast; MFD, moisture flux divergence; PW, precipitable water.

coupling between these deficiencies is evidenced as a drop in low-level moisture flux convergence in the NCEP and ARPEGE-Tropiques analyses (near 12.5°N) and moisture divergence in the ECMWF system (near 13.5°N) during the monsoon season. This feature is thought to play a major role in the southward blocking of the rainbelt.

[51] This work stresses the importance of improving physical parameterizations of moist processes and the treatment of interactions between the surface and the atmosphere in NWP systems over West Africa. In that respect, the AMMA field campaign of 2006 and the considerable research effort that followed represent a significant step forward (see the huge list of publications that came out recently, e.g., in the special issues of the *Journal of Hydrology*, the *Quarterly Journal of the Royal Meteorological Society*, and *Weather Forecasting*). Further improvements in the quality of NWP analyses and forecasts are also expected from the correction radiosonde humidity biases [*Agustí-Panareda et al.*, 2010], the assimilation of new satellite data providing information on lower-tropospheric humidity over land [*Karbou et al.*, 2009; *Bauer*, 2009] and the improvement of soil moisture schemes [*Balsamo et al.*, 2009]. The hybrid water budget data set developed in part 1 of this study [*Meynadier et al.*, 2010] and the GPS PWV observations are also expected to provide insight into smaller spatial and temporal scales of relevance for the investigation of the water cycle and the improvement of moist processes in NWP systems.

Appendix A: Assessment of NWP Model Water Budget Errors

[52] Here operational analyses (AN) and forecasts (FC) from ECMWF-IFS over the period of 1 May to 30 September 2006 are used to assess budget closure issues and computational errors typical of NWP models. The FC fields are extracted for lead times of +12 to +36 hours, valid between 0000 UTC and 2400 UTC, each day. Daily mean quantities are computed between 0000 UTC of one day and 0000 UTC of the next day. First, we use gridded fields at the full resolution of the model, with a horizontal mesh of 0.25° × 0.25° and 91 vertical levels between the surface and 0.1 hPa. In this case, MFD is computed from model levels comprised between the surface and ~100 hPa (55 hybrid levels). Then, we use the fields interpolated on pressure level with two different horizontal grid meshes (0.25° × 0.25° and 2.5° × 2.5°) in order to evaluate the impact of vertical and horizontal resolution on MFD computations. In this case, only 10 pressure levels are available, between 1000 and 100 hPa. The 5 month average results are presented in Figure A1 and Tables A1–A4.

[53] Figure A1a shows that dPW_{FC} exhibits large positive and negative values, locally up to ± 2 mm d^{-1}. Table A1 reports values for box averages, with dPW_{FC} = +0.39 mm d^{-1} in the GUI and +0.65 mm d^{-1} in the SOU box. These represent unrealistic increase in PWV of ~100 kg m^{-2} over 5 months. Such systematic drifts in the model reveal inconsistencies between the model physics and observations. In contrast, dPW_{AN} shows values smaller than ± 0.25 mm d^{-1} everywhere (Figure A1), with box-averaged values ranging between 0.01 and 0.09 mm d^{-1}, i.e., +1.5–14 kg m^{-2} over 5 months (Table A1). Figures A1a and A1b show that the standard deviations of daily fluctuations in dPW are locally on the order of 6 mm d^{-1}. The box-averaged daily standard deviations are significantly reduced, with values between 1.8 and 2.6 mm d^{-1} (Table A2). In contrast to the mean values, which exhibit large biases between dPW_{FC} and dPW_{AN}, the daily fluctuations are fairly consistent between AN and FC tendencies, as confirmed from the high correlations in Table A2 (e.g., r = 0.88 in the SAH box).

[54] Table A3 provides an independent evaluation of dPW_{FC} and dPW_{AN} using GPS data at six sites (see Figure A1b for their locations). The mean values of dPW_{AN} are fairly consistent (within one or two standard deviations, cf. to the ±1 σ values indicated next to the GPS mean values) with dPW_{GPS} whereas dPW_{FC} differs significantly from dPW_{GPS} (the differences are larger than 3σ, i.e., significant at more than 99%). Large departures are observed at the locations of Niamey, dPW_{FC} = 0.92 mm d^{-1}, and Tombouctou, dPW_{FC} = $^{-}$0.51 mm d^{-1}, where dPW_{FC} takes very unrealistic values (see also Figure A1). Standard deviations of dPW_{AN} and dPW_{FC} are systematically smaller than observed (middle

Table A2. Same as Table A1, but for Standard Deviations and Correlations of Daily Quantities[a]

Box	dPW_{FC}	dPW_{AN}	Diff (dPW)	Corr (dPW)	MFD_{FC}	MFD_{AN}	Diff (MFD)	Corr (MFD)	Res_{FC}	Res_{AN}
SAH	2.6	2.6	1.3	0.88	2.8	2.8	1.2	0.90	0.53	1.21
SOU	2.0	2.0	1.4	0.75	2.7	2.7	1.8	0.77	0.51	1.88
GUI	1.8	1.9	1.3	0.75	3.3	3.5	2.4	0.76	0.83	3.14

[a]Diff is the temporal standard deviation of the difference between forecast (FC) and analysis (AN) terms, and Corr is the correlation between time series of daily FC and AN terms.

Table A3. Statistics of Daily PWV Tendency Computed From GPS PWV Data, ECMWF-IFS Forecast and Analysis, May–September 2006, at the Location of Six GPS Stations[a]

Station	Latitude (°N)	Mean			Standard Deviation			Correlation	
		GPS	AN	FC	GPS	AN	FC	r(GPS.AN)	r(GPS.FC)
TOMB	16.7	0.02 ± 0.05	−0.02	−0.51	6.9	6.2	5.5	0.59	0.49
GAO1	16.3	0.09 ± 0.05	0.09	0.26	7.4	6.7	6.6	0.74	0.78
NIAM	13.5	0.32 ± 0.05	0.26	0.92	6.6	6.3	4.9	0.87	0.55
OUAG	12.5	0.05 ± 0.05	0.04	0.42	6.3	4.8	5.1	0.75	0.54
DJOU	9.7	−0.01 ± 0.03	0.03	0.12	4.8	4.5	3.9	0.54	0.30
TAMA	9.6	0.03 ± 0.04	0.02	0.32	5.7	4.1	4.0	0.68	0.50
Average		**0.08 ± 0.08**	**0.07**	**0.25**	**6.3**	**5.4**	**5.0**	**0.69**	**0.53**

[a]PWV tendency is in units of mm d^{-1}. Abbreviations are as follows: AN, analysis; ECMWF, European Centre for Medium-Range Weather Forecasts; FC, forecast; IFS, Integrated Forecasting System; PWV, precipitable water vapor.

section of Table A3) but correlations (rightmost section of Table A3) are fair (0.69 for AN and 0.53 for FC, on average).

[55] Figures A1c and A1d show MFD_{FC} and MFD_{AN} as computed from model-level q and V fields using equation (1). Both estimates suffer from similar computational errors: (1) the finite difference scheme used for the computation of horizontal wind divergence from gridded wind fields and (2) the time sampling error due to the use of 6 hourly instead of cumulated q and V data. Hence, the differences observed between MFD_{FC} and MFD_{AN} here are supposed to be representative of difference in the AN and FC fields (i.e., revealing the impact of analysis increments). The mean fields reveal slightly different patterns, mainly MFD_{AN} shows large zones of increased convergence to the north (15°N–20°N) and to the south (5°N–10°N). They result in slightly different box-averaged mean values (mostly in the GUI box; see Table A1). The daily fluctuations are fairly consistent, with standard deviations reaching 10 mm d^{-1}, locally (Figures A1c and A1d) and 2.8–3.5 mm d-^{1} for the box averages (Table A2). The linear correlation coefficient between daily MFD_{FC} and MFD_{AN} estimates is rather high (0.76 in the GUI box to 0.90 in the SAH box).

[56] The comparisons above give insight into the difference between the AN and FC fields, but the MFD_{FC} and MFD_{AN} estimates contain computational errors. An evaluation of these errors is provided here comparing $MFD_{FC,cumul} = E_{FC} - P_{FC} - dPW_{FC}$ with MFD_{FC}. Indeed, $MFD_{FC,cumul}$ is an estimate of MFD_{FC} using the residual approach which avoids direct computation errors. Figure A1e shows that $MFD_{FC,cumul}$ is much smoother than MFD_{FC}. The spatial patterns of the mean quantity are less noisy and the temporal variability is reduced from 10 mm d^{-1} to 6 mm d^{-1}, locally. Figure A1g shows also the mean and standard deviation of daily differences. Locally, biases of up to ± 2 mm d^{-1} are seen and the standard deviation of differences reaches 8 mm d^{-1}. The box-averaged differences are reported in Tables A1 and A2 as $Res_{FC} = MFD_{FC} - MFD_{FC,cumul}$. Both the mean errors and the standard deviations are small (−0.1/0.2 mm d^{-1} for mean error and 0.51–0.83 mm d^{-1} for standard deviations). This result is important as Res_{FC} is also representative of the misclosure between FC budget terms: $Res_{FC} = MFD_{FC} - (E_{FC} - P_{FC} - dPW_{FC})$. Hence, this confirms that $dPW_{FC} + MFD_{FC} \approx (E_{FC} - P_{FC})$ when the terms are averaged over boxes of ~10^6 km^2.

[57] The fact that the budget between FC terms is closed does not, however, guarantee that the balance between the terms is correct. It is shown above that dPW_{FC} is biased in comparison to dPW_{GPS} and dPW_{AN}. Similarly, MFD_{FC} is biased compared to MFD_{AN}, and in addition $E_{FC} > P_{FC}$ (Table A1), which is the opposite of what was found from the hybrid data set [*Meynadier et al.*, 2010]. Hence, it is not surprising that the budget is no longer closed when $dPW_{FC} + MFD_{FC}$ is replaced with $dPW_{AN} + MFD_{AN}$. The residual, Res_{AN} in Table A1 which is equivalent to $Res_a = (dPW_{AN} + MFD_{AN}) - (E_{FC} - P_{FC}) = (dPW_{AN} + MFD_{AN}) - (dPW_{FC} + MFD_{FC,\ cumul})$, is an estimate of the overall analysis increment combined with the computation errors. It is negative in all three boxes (e.g., −1.42 mm d^{-1} in the GUI box) which is a result of the discrepancy both between dPW_{AN} and dPW_{FC}, and between MFD_{AN} and $MFD_{FC,\ cumul}$, with nearly similar weight (Table A1). The comparison of Res_{AN} and Res_{FC} indicates that analysis increments are dominating computation errors for box-averaged terms (Table A1).

[58] The impact of limited vertical and horizontal resolutions on MFD computations are also quantified in Figures A1f and A1h. The former estimates MFD_{PL}, computed from 10 pressure levels at 0.25° × 0.25°. Comparing this estimate to the full model level estimate, MFD_{ML} (Figure A1d), shows that: convergence is enhanced to the north; divergence is enhanced in the central region; divergence-convergence dipoles appear to the south, near the coast, and in the mountainous areas. The temporal variability is also enhanced from 10 mm d^{-1} to 12 mm d^{-1}, locally. The reverse is observed from the coarser resolution fields (Figure A1h). The inspection of vertical structure of

Table A4. Synthesis of the Main Uncertainties Affecting the Water Budget Computations With ECMWF-IFS: The Analysis Increment, $(dPW_{AN} + MFD_{AN}) - (dPW_{FC} + MFD_{FC})$, the Error in MFD Due to Time Sampling and Finite Difference Approximation of the Divergence Operator, $(MFD_{FC} - MFC_{FC,cumul})$, and the Error in MFD Due to Vertical Sampling, $(MFD_{PL} - MFD_{ML})$[a]

RMSE	Analysis Increment	Time Sampling + Finite Difference Divergence Computation	Vertical Resolution (10 Pressure Levels, Full Model Levels)
SAH	−1.12 ± 0.43	−0.14 ± 0.34	0.97 ± 0.48
SOU	−0.93 ± 0.53	−0.16 ± 0.26	−0.12 ± 0.33
GUI	−1.64 ± 0.30	0.23 ± 0.33	−0.31 ± 0.36

[a]The values are mean ±1 standard deviation of monthly quantities over the period May–September 2006. Units are mm d^{-1}. Abbreviations are as follows: ECMWF-IFS, European Centre for Medium-Range Weather Forecasting Integrated Forecasting System; MFD, moisture flux divergence; MFC, moisture flux convergence.

wind fields and MFD (Figures 9 and 10) reveals that the complex structure and vertical shear of the horizontal wind components over West Africa is poorly represented with 10 pressure levels only, especially in the vicinity of the low-level jet and the AEJ.

[59] Table A4 provides a synthesis of estimates of the three main error sources in the daily water budget terms computed from ECMWF-IFS model: the analysis increment, $(dPW_{AN} + MFD_{AN}) - (dPW_{FC} + MFD_{FC})$, the time sampling and divergence computational errors, $(MFD_{FC,\ cumul} - MFD_{FC})$, and the vertical undersampling error (10 pressure levels versus full hybrid model levels).

[60] **Acknowledgments.** On the basis of a French initiative, AMMA was built by an international scientific group and is currently funded by a large number of agencies, especially from France, the United Kingdom, the United States, and Africa. It has been the beneficiary of a major financial contribution from the European Community's Sixth Framework Research Programme. Detailed information on scientific coordination and funding is available on the AMMA International Web site (http://www.amma-international.org/). The authors would like to thank Marie-Noelle Bouin for processing the GPS data, Aaron Boone for providing the ALMIP data set, Sophie Cloché for providing the NWP model products, and Steven Ghan and the two anonymous reviewers for useful comments that helped improve this paper.

References

Agustí-Panareda, A., et al. (2009), Radiosonde humidity bias correction over the West African region for the special AMMA reanalysis at ECMWF, *Q. J. R. Meteorol. Soc.*, *135*, 595–617, doi:10.1002/qj.396.

Agustí-Panareda, A., A. Beljaars, C. Cardinali, I. Genkova, and C. Thorncroft (2010), Impact of assimilating AMMA soundings on ECMWF analyses and forecasts, *Weather Forecast.*, doi:10.1175/2010WAF2222370.1, in press.

Andersson, E., et al. (2005), Assimilation and modeling of the atmospheric hydrological cycle in the ECMWF forecasting system, *Bull. Am. Meteorol. Soc.*, *86*, 387–402, doi:10.1175/BAMS-86-3-387.

Balsamo, G., P. Viterbo, A. Beljaars, B. van den Hurk, M. Hirschi, A. K. Betts, and K. Scipal (2009), A revised hydrology for the ECMWF model: Verification from field site to terrestrial water storage and impact in the Integrated Forecast System, *J. Hydrometeorol.*, *10*, 623–643, doi:10.1175/2008JHM1068.1.

Bauer, P. (2009), 4D-Var assimilation of MERIS total column water-vapour retrievals over land, *Q. J. R. Meteorol. Soc.*, *135*, 1852–1862, doi:10.1002/qj.509.

Bechtold, P., M. Köhler, T. Jung, F. Doblas-Reyes, M. Leutbecher, M. J. Rodwell, F. Vitart, and G. Balsamo (2008), Advances in simulating atmospheric variability with the ECMWF models: From synoptic to decadal time-scales, *Q. J. R. Meteorol. Soc.*, *134*, 1337–1351, doi:10.1002/qj.289.

Betts, A. K., J. H. Ball, and P. Viterbo (1999), Basin-scale surface water and energy budgets for the Mississippi from the ECMWF reanalysis, *J. Geophys. Res.*, *104*, 19,293–19,306, doi:10.1029/1999JD900056.

Bielli, S., and R. Roca (2009), Scale decomposition of atmospheric water budget over West Africa during the monsoon 2006 from NCEP/GFS analyses, *Clim. Dyn.*, *35*, 143–157, doi:10.1007/s00382-009-0597-5.

Bock, O., and M. Nuret (2009), Verification of NWP model analyses and radiosonde humidity data with GPS precipitable water vapor estimates during AMMA, *Weather Forecast.*, *24*, 1085–1101, doi:10.1175/2009WAF2222239.1.

Bock, O., M.-N. Bouin, A. Walpersdorf, J. P. Lafore, S. Janicot, F. Guichard, and A. Agusti-Panareda (2007), Comparison of ground-based GPS precipitable water vapour to independent observations and numerical weather prediction model reanalyses over Africa, *Q. J. R. Meteorol. Soc.*, *133*, 2011–2027, doi:10.1002/qj.185.

Bock, O., et al. (2008), West African Monsoon observed with ground-based GPS receivers during African Monsoon Multidisciplinary Analysis (AMMA), *J. Geophys. Res.*, *113*, D21105, doi:10.1029/2008JD010327.

Boone, A., et al. (2009a), The AMMA Land Surface Model Intercomparison Project (ALMIP), *Bull. Am. Meteor. Soc.*, *90*, 1865–1880, doi:10.1175/2009BAMS2786.1.

Boone, A., I. Poccard-Leclercq, Y. Xue, J. Feng, and P. de Rosnay (2009b), Evaluation of the WAMME model surface fluxes using results from the AMMA land-surface model intercomparison project, *Clim. Dyn.*, *35*, 127–142, doi:10.1007/s00382-009-0653-1.

Brubaker, K. L., D. Entekhabi, and P. S. Eagleson (1993), Estimation of continental precipitation recycling, *J. Clim.*, *6*, 1077–1089, doi:10.1175/1520-0442(1993)006<1077:EOCPR>2.0.CO;2.

Cadet, D. L., and O. Nnoli (1987), Water vapour transport over Africa and the Atlantic Ocean during summer 1979, *Q. J. R. Meteorol. Soc.*, *113*, 581–602, doi:10.1002/qj.49711347609.

Descroix, L., et al. (2009), Spatio-temporal variability of hydrological regimes around the boundaries between Sahelian and Sudanian areas of West Africa: A synthesis, *J. Hydrol. Amsterdam*, *375*, 90–102, doi:10.1016/j.jhydrol.2008.12.012.

Drusch, M., and P. Viterbo (2007), Assimilation of screen-level variables in ECMWF's Integrated Forecast System: A study on the impact on the forecast quality and analyzed soil moisture, *Mon. Weather Rev.*, *135*, 300–314, doi:10.1175/MWR3309.1.

Ebisuzaki, W. (1997), A method to estimate the statistical significance of a correlation when the data are serially correlated, *J. Clim.*, *10*, 2147–2153, doi:10.1175/1520-0442(1997)010<2147:AMTETS>2.0.CO;2.

Faccani, C., F. Rabier, N. Fourrié, A. Agustí-Panareda, F. Karbou, P. Moll, J.-P. Lafore, M. Nuret, F. Hdidou, and O. Bock (2009), The impact of the AMMA radiosonde data on the French global assimilation and forecast system, *Weather Forecast.*, *24*, 1268–1286, doi:10.1175/2009WAF2222237.1.

Fontaine, B., P. Roucou, and S. Trzaska (2003), Atmospheric water cycle and moisture fluxes in the West African Monsoon: Mean annual cycles and relationship using NCEP/NCAR reanalysis, *Geophys. Res. Lett.*, *30*(3), 1117, doi:10.1029/2002GL015834.

Gong, C., and E. A. B. Eltahir (1996), Sources of moisture for rainfall in West Africa, *Water Resour. Res.*, *32*, 3115–3121, doi:10.1029/96WR01940.

Guichard, F., et al. (2010), An intercomparison of simulated rainfall and evapotranspiration associated with a mesoscale convective system over West Africa, *Weather Forecast.*, *25*, 37–60, doi:10.1175/2009WAF2222250.1.

Higgins, R. W., K. C. Mo, and S. D. Schubert (1996), The moisture budget of the central United States in spring as evaluated in the NCEP/NCAR and the NASA/DAO reanalyses, *Mon. Weather Rev.*, *124*, 939–963, doi:10.1175/1520-0493(1996)124<0939:TMBOTC>2.0.CO;2.

Hourdin, F., et al. (2010), AMMA-Model Intercomparison Project, *Bull. Am. Meteorol. Soc.*, *91*, 95–104, doi:10.1175/2009BAMS2791.1.

Huffman, G. J., et al. (2007), The TRMM Multisatellite Precipitation Analysis (TMPA): Quasi-global, multiyear, combined-sensor precipitation estimates at fine scales, *J. Hydrometeorol.*, *8*, 38–55, doi:10.1175/JHM560.1.

Janicot, S., et al. (2008), Large-scale overview of the summer monsoon over West Africa during the AMMA field experiment in 2006, *Ann. Geophys.*, *26*, 2569–2595, doi:10.5194/angeo-26-2569-2008.

Kalnay, E., et al. (1996), The NCEP/NCAR 40-Year Reanalysis Project, *Bull. Am. Meteorol. Soc.*, *77*, 437–471, doi:10.1175/1520-0477(1996)077<0437:TNYRP>2.0.CO;2.

Kanamitsu, M., and S. Saha (1996), Systematic tendency error in budget calculations, *Mon. Weather Rev.*, *124*, 1145–1160, doi:10.1175/1520-0493(1996)124<1145:STEIBC>2.0.CO;2.

Kanamitsu, M., W. Ebisuzaki, J. Woolen, J. Potter, and M. Fiorino (2002), NCEP/DOE AMIP II Reanalysis (R-2), *Bull. Am. Meteorol. Soc.*, *83*, 1631–1643, doi:10.1175/BAMS-83-11-1631(2002)083<1631:NAR>2.3.CO;2.

Karbou, F., F. Rabier, J.-P. Lafore, J.-L. Redelsperger, and O. Bock (2009), Global 4D-Var assimilation and forecast experiments using land surface emissivities from AMSU-A and AMSU-B. Part II: Impact of adding surface channels on the African Monsoon during AMMA, *Weather Forecast.*, *25*, 20–36, doi:10.1175/2009WAF2222244.1.

Lamb, P. J. (1983), West African water vapor variations between recent contrasting sub-Saharan rainy seasons, *Tellus, Ser. A*, *35*, 198–212, doi:10.1111/j.1600-0870.1983.tb00197.x.

Lebel, T., et al. (2009), The AMMA field campaigns: Multiscale and multidisciplinary observations in the West African region, *Q. J. R. Meteorol. Soc.*, *136*, 8–33, doi:10.1002/qj.486.

Lothon, M., F. Saïd, F. Lohou, and B. Campistron (2008), Observation of the diurnal cycle in the low troposphere of West Africa, *Mon. Weather Rev.*, *136*, 3477–3500, doi:10.1175/2008MWR2427.1.

Maurer, E. P., G. M. O'Donnell, D. P. Lettenmaier, and J. O. Roads (2001), Evaluation of the land surface water budget in NCEP/NCAR and NCEP/DOE reanalyses using an off-line hydrologie model, *J. Geophys. Res.*, *106*, 17,841–17,862, doi:10.1029/2000JD900828.

Meynadier, R., O. Bock, F. Guichard, A. Boone, P. Roucou, and J.-L. Redelsperger (2010), West African Monsoon water cycle: 1. A hybrid water budget data set, *J. Geophys. Res.*, *115*, D19106, doi:10.1029/2010JD013917.

Nicholson, S. E., J. Kim, M. B. Ba, and A. R. Lare (1997), The mean surface water balance over Africa and its interannual variability,

J. Clim., *10*, 2981–3002, doi:10.1175/1520-0442(1997)010<2981:TMSWBO>2.0.CO;2.

Nuret, M., J.-P. Lafore, N. Ascencio, H. Benichou, O. Bock, F. Favot, T. Montmerle, and Y. Seity (2007), Evaluation of Meteo-France numerical weather prediction models during AMMA 2006-SOP, *ALADIN Newsl.*, *32*, 93–107.

Nuret, M., J.-P. Lafore, O. Bock, F. Guichard, A. Agusti-Panareda, J.-B. Ngamini, and J.-L. Redelsperger (2008), Correction of humidity bias for Vaïsala RS80 sondes during AMMA 2006 observing period, *J. Atmos. Oceanic Technol.*, *25*, 2152–2158, doi:10.1175/2008JTECHA1103.1.

Parker, D. J., R. R. Burton, A. Diongue-Niang, R. J. Ellis, M. Felton, C. M. Taylor, C. D. Thorncroft, P. Bessemoulin, and A. M. Tompkins (2005), The diurnal cycle of the West African Monsoon circulation, *Q. J. R. Meteorol. Soc.*, *131*, 2839–2860, doi:10.1256/qj.04.52.

Parker, D. J., et al. (2008), The AMMA Radiosonde Program and its implications for the future of atmospheric monitoring over Africa, *Bull. Am. Meteorol. Soc.*, *89*, 1015–1027, doi:10.1175/2008BAMS2436.1.

Peyrillé, P., J.-P. Lafore, and J.-L. Redelsperger (2007), An idealized two-dimensional framework to study the West African Monsoon. Part I: Validation and key controlling factors, *J. Atmos. Sci.*, *64*, 2765–2782.

Roads, J. (2003), The NCEP-NCAR, NCEP-DOE, and TRMM tropical atmosphere hydrologic cycles, *J. Hydrometeorol.*, *4*, 826–840, doi:10.1175/1525-7541(2003)004<0826:TNNATT>2.0.CO;2.

Roads, J., M. Kanamitsu, and R. Stewart (2002), CSE water and energy budgets in the NCEP-DOE Reanalysis II, *J. Hydrometeorol.*, *3*, 227–248, doi:10.1175/1525-7541(2002)003<0227:CWAEBI>2.0.CO;2.

Simmons, A., S. Uppala, D. Dee, and S. Kobayashi (2006), ERA-Interim: ECMWF reanalysis products from 1989 onwards, *ECMWF Newsl.*, *110*, 25–35.

Sultan, B., and S. Janicot (2000), Abrupt shift of the ITCZ over West Africa and intra-seasonal variability, *Geophys. Res. Lett.*, *27*, 3353–3356, doi:10.1029/1999GL011285.

Tompkins, A. M., A. Diongue-Niang, D. J. Parker, and C. D. Thorncroft (2005), The African easterly jet in the ECMWF Integrated Forecast System: 4D-Var analysis, *Q. J. R. Meteorol. Soc.*, *131*, 2861–2885.

Trenberth, K. E. (1991), Climate diagnostics from global analyses: Conservation of mass in ECMWF analyses, *J. Clim.*, *4*, 707–722, doi:10.1175/1520-0442(1991)004<0707:CDFGAC>2.0.CO;2.

Trenberth, K. E., and C. J. Guillemot (1995), Evaluation of the global atmospheric moisture budget as seen from Analyses, *J. Clim.*, *8*, 2255–2272, doi:10.1175/1520-0442(1995)008<2255:EOTGAM>2.0.CO;2.

Trenberth, K. E., and C. J. Guillemot (1998), Evaluation of the atmospheric moisture and hydrologic cycle in the NCEP/NCAR reanalyses, *Clim. Dyn.*, *14*, 213–231, doi:10.1007/s003820050219.

Trenberth, K. E., and L. Smith (2009), The three dimensional structure of the atmospheric energy budget: Methodology and evaluation, *Clim. Dyn.*, *32*, 1065–1079, doi:10.1007/s00382-008-0389-3.

Zhang, C., D. S. Nolan, C. D. Thorncroft, and H. Nguyen (2008), Shallow meridional circulations in the tropical atmosphere, *J. Clim.*, *21*, 3453–3470, doi:10.1175/2007JCLI1870.1.

A. Agustí-Panareda and A. Beljaars, ECMWF, Shinfield Park, Reading RG2 9AX, UK.

O. Bock, S. Gervois, and R. Meynadier, LATMOS, Université Pierre et Marie Curie, Tour 45, Couloir 45-46, Boite 102, 4, pl. Jussieu, F-75252 Paris CEDEX 05, France. (olivier.bock@latmos.ipsl.fr)

F. Guichard and J.-L. Redelsperger, GAME-CNRM, Météo-France, 42, ave. Gaspard Coriolis, F-31057 Toulouse CEDEX 01, France.